THE CHARACTERIZATION OF FRIABLE SURFACE DEPOSISTS ACROSS NORTH AFRICA UTILIZING COMPUTER CONTROLLED SCANNING ELECTRON MICROSCOPY (CCSEM)

by

ZACHARY EDWARD SUTTON

Presented to the Faculty of the Graduate School of

The University of Texas at Arlington in Partial Fulfillment

of the Requirements

for the Degree of

MASTER OF SCIENCE IN EARTH AND ENVIRONMENTAL SCIENCES

THE UNIVERSITY OF TEXAS AT ARLINGTON

May 2016

Acknowledgements

This thesis could not have been completed without the assistance of several individuals. First off, I would like to thank my thesis advisor Dr. Andrew Hunt for both his time and mentorship throughout this entire process. Additionally, I would like to thank the committee members Dr. James Grover and Dr. John Wickham for their time and patience. Thank you Dr. Frank Oldfield and Richard Lyons from the University of Liverpool for providing the samples, which were analyzed. I would also like to thank Zakariah Sabatka for his assistance in this thesis and for his career guidance.

April 14, 2016

Abstract

THE CHARACTERIZATION OF FRIABLE SURFACE DEPOSISTS ACROSS NORTH AFRICA UTILIZING COMPUTER CONTROLLED SCANNING ELECTRON MICROSCOPY (CCSEM)

Zachary Edward Sutton, MS

The University of Texas at Arlington, 2016

Supervising Professor: Andrew Hunt

Analysis of the mineral constituents of friable surface deposits from the Burkina Faso and Niger regions, North Africa, was undertaken by computer controlled scanning electron microscopy (CCSEM) to try and identify variations in mineralogical composition which could be used for source attribution to distinguish windblown material from different contributing source areas. A total of 16 friable surface samples were collected for CCSEM analysis. These samples were from multiple geographic locations within the Burkina Faso region. CCSEM analysis generated data on individual dust particles that included: particle size, shape, and chemical composition. This combination of the Scanning Electron Microscope (SEM) working in the Backscattered Electron Imaging (BEI) mode was used for the aforementioned particle characterization. The BEI mode of imaging of microscopic dust particles provided information on the average atomic number composition and particle morphology. The use of a Silicon Drift X-ray detector with an ultra-thin window provided all element data on individual particles.

The principal goal of this project was to (1) compare and contrast surface material from laterites versus proximal soils from the Burkina Faso and Niger regions of North Africa with the intention of differentiating the material from each other at the individual particle level and (2) to establish a linear classification scheme based upon the mineral composition of North African surface sediments to permit the attribution of laterite and soil particles to specific mineral classes. The mineralogy of the individual particles from all soil samples was determined by CCSEM. CCSEM analysis provided data on thousands of particles and, as a result, significant sized data sets can be evaluated statistically.

With friable soil particles it is commonly of no use in CCSEM analysis to define specific mineral particle types. Obdurate minerals such as quartz may often be identified in CCSEM data (Particles composed wholly of Si). Unfortunately, transformation processes, such as the particles being coated by Fe, alter the composition of basic mineral forms in regards to the chemical composition identified in the SEM. In

order to provide a realistic classification of the particles analyzed here, a reference data set from the analysis of a North African friable surface deposits sample was used to develop a classification scheme. Homogenous groups of particles within the data set were identified with the use of assisted cluster analysis. Homogenous groups of particles were distinguished based upon the associations of constituent particle elements. A 59-class element-based classification scheme was then developed based upon the homogenous groups identified. All classes were listed in a linear sorting order which was used to classify the CCSEM data from the soil samples collected within this study. The study sample CCSEM analysis typically contained element and other data on approximately 5,100 particles per sample.

Table of Contents

List of Illustrations

List of Tables

Chapter 1

Introduction

Trade winds are known to be of significant influence in regards to the deposition of dusts and fine sediments. Eolian erosion and deposition processes, such as the Trans-Atlantic trade winds, have redistributed fine surface sediments from Africa across the Atlantic Ocean to the Americas. Unfortunately, the exact amount or percentage of African surface sediment transported remains unknown. In addition, diagenesis of the sediment via chemical and physical alterations may have occurred during the transportation process. Alterations may be influenced by the duration which the sediment spends in the atmosphere and may possess the potential to absorb pollutants such as chlorine, sulphates, and organics (Sullivan et al., 2007; Falkovich et al., 2004; Mamane et al., 1980). Once deposited, the sediments could initiate allergy issues for both children and susceptible adults. (Goudie and Midddleton, 2001; Prospero, 1999; Prospero et al., 1981; Mahowald et al., 2005; Mather et al., 2008). Currently, the exact number of asthma hospitalizations which have been the result reactions with African sediments remains uncertain.

Furthermore, nutrient contribution for Central and South American forests are believed to influenced by the aforementioned eolian sediments and atmospheric dusts, precise amounts contributed remain unknown though (Bartholet, 2012). The soils of the Amazon basin are consistently bombarded and eroded due to heavy rainfalls which deplete these soils of nutrients, and for that reason, African dusts likely serve as a source of nutrient replenishment. South American surface sediments a relatively high iron content, vital for vegetation within the region, but unfortunately the high iron content could cause damage to ocean ecosystems as a result of the addition of anthropogenic pollutants (Bartholet, 2012). One study into the effect of iron and anthropogenic pollutants indicated that iron transported in the atmosphere could possess the potential to bond with ambient acids in the atmosphere, and caused iron particles to be more soluble and therefore increased the amount of available iron in the ocean (Bartholet, 2012).

Lastly, a tertiary effect of African dusts would be their impact upon climate from resultant balance changes between solar and thermal radiation (IPCC, 2007). The total extent of the effects of aerosolized dusts upon chemical reactions in the atmosphere remains (Formenti, et al., 2011). Due to the aforementioned effects of atmospheric dusts as potential hazards, sources of nutrient replenishment, and their influence upon

global climate, accurate characterization and identification of surface sediments provenance remains crucial in understanding the surface sediment creation as well as the diagenetic changes which may occur while transported, thus the motivator to develop an accurate and concise initial elemental and chemical analysis.

Chapter 2

Previous Research

Research on laterite formation has been conducted in various regions around the world. One such study by Dr. Stephen A. Norton found that laterite formation was the result of chemical weathering of a protore, or metalliferous soil or parent rock, by relatively acidic waters thus allowing for the mobilization and leaching of silicate minerals causing the resultant rock to have increased ratios of either Fe, Al, or Fe and Al (Norton, 1973). More specific to the Burkina Faso Region, sampling and analysis of laterites from the Balkouin area of Burkina Faso was conducted in 2013 (Giorgis et al., 2013). Inductively coupled plasma (ICP) atomic emission spectrometry (AES) and mass spectrometry (MS) were combined to characterize the major elements which compose laterites. The analysis determined that the 12 basic elements comprise laterites were Si, Ti, Al, Fe, Mn, Mg, Ca, Na, K, P, Cr, and O. Of the aforementioned 12 elements Si, Al, and Fe accounted for between 81 – 91% of the lateritic profile (Giorgis et al., 2013).

Previous research has also shown that the transportation of surface sediments from North and Central African and deposition to the Iberian Peninsula has occurred and predominately consisted of calcite-dolomite, silica, but did contain minor amounts of micas, feldspars, gypsum and other trace minerals (Avila et al., 1997; Coz et al., 2009). Scanning Electron Microscope coupled with Energy Dispersive X-ray Spectroscopy (SEM/EDS) was used to characterize 11 basic elements and the mineral content of dust provenance via elemental analysis. The 11 elements were then clustered together in various combinations in order to generate sample classes which would enable the segregation of the particles. Results showed that, in general, dust samples from Madrid consisted of between 65 - 85% silica. Subsequently, it is believed that North African surface sediments may be the cause of the relative high abundance of silicates in the dusts collected from the Iberian Peninsula.

In conjunction with chemical analysis, Aspect Ratios (AR) were used to evaluate and compare particle morphology to estimate the probability of particle transportation in the atmosphere and to attempt to

determine the provenance of the dust itself. A determination was reached that particle deposition occurred due to three mechanisms, impaction, sedimentation and Brownian diffusion (Morman and Plumlee, 2013). Gravitation sedimentation was a significant factor for particles with a diameter larger than 0.5 μm as the distance of particle transportation is limited, whereas diffusional transport appeared to govern the transportation for particles with a diameter less than 0.5 μm where minor displacements are the result of the collision between gas molecules and particles (Shultz et al, 2000). Additionally, surface sediments from the Sahel region were comprised of enhanced secondary ferromagnetic minerals which suggested that the concentration of fine-grained clay fraction (<2 μm) had a tenfold difference between the arid north and the humid south of Niger, and there was also a less significant statistical correlation for hematite concentrations and rainfall across the region (Lyons et al, 2010). Certain surface sediments from the Benin and southern Togo region exhibited magnetic properties inconsistent with their associated parent rocks. Thus, researchers concluded that climate variations did play a pivotal role in source locations of African dusts. Additional collection and characterization, particle separation, and chemical analysis will be required in order to achieve a better understanding of how climate variations effect the distribution of African dusts (Lyons et al, 2010).

Preliminary research was conducted by Dr. Joseph Prospero at the University of Miami. Samples of dusts were collected from the Florida Keys, Bahamas, and the Amazon. The determination was reached that the Earth annually emitted approximately two billion metric tons of dust with more than half of that being originated from Africa. Other sources state that approximately 40 million metric tons of the aforementioned dusts consisted of iron and phosphates which could potentially travel up to 6400 km across the Atlantic Ocean to the Americas and half of the dusts were originated from the Bodele depression in Africa (Bartholet, 2012). To make it possible for African dusts to cross the Atlantic, a wind speed of approximately 4-12 meters per second was required. Two main effects of the global transportation of dusts upon the Earth's climate are known. Firstly, dusts transported in the air could

potentially increase a region's albedo due to their reflective nature. Secondly, dusts effect climate variation as an indirect result from cloud formation. Cloud formation require that water droplets form around a condensation nucleus, such as dust, and as a result may either increase or decrease the temperatures and amount of rainfall within a region's climate (Bartholet, 2012).

Studies on eolian transportation and deposition have revealed that there is a link between inorganic mineral dusts and the overall health of the population (Morman and Plumlee, 2013). Limited research has been conducted on source characterizations and subsequently has caused difficulties in quantifying the health effects of long range transportation of dust (Morman and Plumlee, 2013). It is estimated that approximately 1.3 million deaths are the result of outdoor air pollution (WHO, 2012a). As defined by the USEPA (2012a), coarse particles are those between 2.5-10 µm in diameter. Additionally, the toxicological effects of dust particles with diameters less than 5 µm are determined by the chemical stability of the particles. At the present time, few studies exist which show a link between inorganic mineral dust and health effects (Morman and Plumlee, 2013). A primary factor which must be determined is the effect of inorganic mineral dust on the population as well as the chemical and physical characteristics of the dust (Plumlee et al, 2006). Increased concern has risen regarding African dusts high silica content which may cause pneumoconiosis, also known as Desert Lung. The increase in desertification from climate changes has made pneumoconiosis a concern for both humans and livestock in arid, dusty regions (Kuehn, 2006). Numerous studies have associated regional dust from sources, such as the Sahel/Saharan region of Africa, with an overall increase in hospitalization and mortality in areas such as Europe (Morman and Plumlee, 2013; Perez et al, 2007). Approximately half of all African dusts are estimated to have a diameter of less than 2.5 µm (Morman and Plumlee, 2013), which would suggest that a significant amount of African dust may be aerosolized and transported across the Atlantic Ocean with relative ease.

Inconsistencies and a lack of data still remain despite the numerous studies which have been conducted on the effects of both short and long range dust transportation, and have led to a conclusion that

additional research remains needed on sample and source characterization, model parameters, and susceptibility (Morman and Plumlee, 2013). Morman and Plumlee (2013) stated, “Much more information regarding source location, sample characterization (biological, mineralogy, and chemistry), emission rates and models, and particle size are needed to understand the implication of exposure and etiological agent(s) responsible.”

Chapter 3

Objectives and Expected Outcomes

This study was conducted with the primary objective of characterizing North African surface soils and laterites from the Burkina Faso region based upon their elemental compositions as revealed in the Scanning Electron Microscope (SEM). In determining a consistent chemical composition in the soils within Burkina Faso and neighboring regions, it was hoped that the determination of dust provenance may be achieved for dust particles from trans-Atlantic winter storms if dust samples were collected post trans-Atlantic transport. It is postulated that the soil and laterite samples from the Burkina Faso region will have unique chemical compositions which may be categorized in this study to be used as an identifier of sediment provenance in subsequent studies. The general consistency of elements within these samples is expected to be comprised of silica, aluminum, iron, and potassium. Data was procured from 15 samples collected between July and September 2007. Latitude and longitudes sample locations is listed in table 3-1. Additionally, all sample locations have been mapped in figure 3-1.

Table 3-1 Samples and sample locations

Site Number	Latitude	Longitude
0	13° 29.809 N	02° 03.770 E
1	13° 31.704 N	02° 03.203 E
2	13° 17.087 N	01° 54.392 E
3	12° 58.308 N	01° 44.449 E
4	12° 43.603 N	01° 37.670 E
5	13° 25.337 N	01° 19.837 E
6	13° 17.087 N	00° 56.326 E
7	12° 03.736 N	00° 23.608 E
8	12° 10.016 N	00° 08.378 E
9	12° 15.016 N	00° 42.725 W
10	12° 21.801 N	01° 03.116 W
11	12° 29.038 N	01° 14.738 W
12	12° 24.672 N	01° 25.207 W

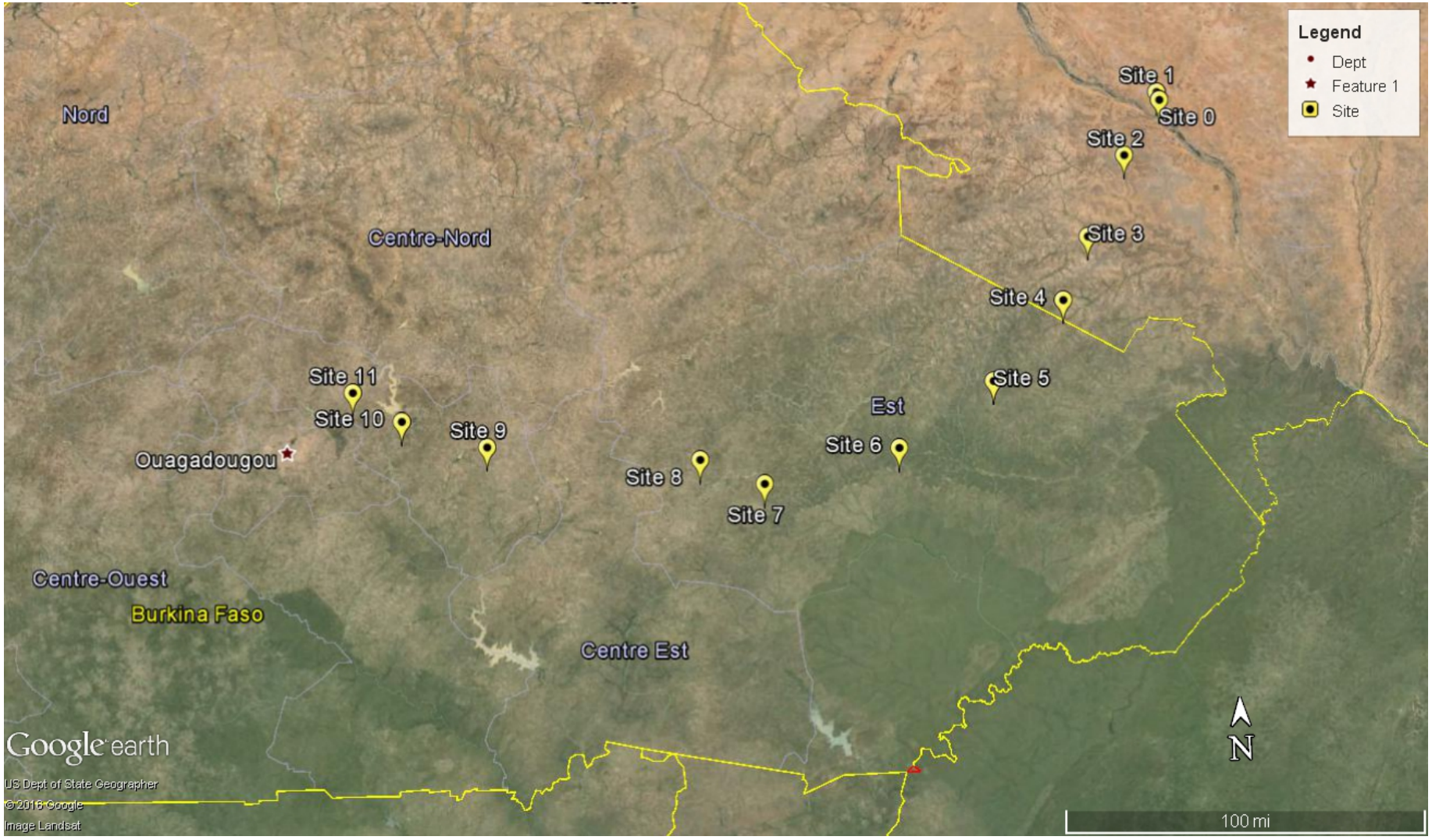

Figure 3-1: Google Earth Map illustrating sample locations within the Burkina Faso and Niger regions.

Chapter 4

Research Design and Procedures

The mineralogical makeup of the 16 sediment samples was characterized by computer controlled SEM analysis (CCSEM). Sediment sample preparation for CCSEM analysis was conducted in the following stages. (1) A portion of the sediment from each sample location was placed in an individual 50 mL test tube containing distilled water to which a minor amount (< 1 ml) of surfactant was added, and then the suspension was ultrasonically agitated for no less than 5 minutes. (2) An aliquot of the sediment water suspension mixture was added to a chimney reservoir prefilled with approximately 20 ml of DI water. The sediment solution was then filtered onto a 25 mm diameter 0.4 µm pore size polycarbonate membrane filter. In order to ensure an optimal sample preparation for CCSEM, the process was repeated and multiple filters were prepared. Sediment samples with approximately one particle diameter separation between particles were preferred for analysis. (3) Each filter was then mounted to a glass laboratory slide with the use of colloidal graphite adhesive.

(a)

(b)

Figure 4-1 (a) Ultrasonic Cleaning System and (b) vacuum and filter system

An ASPEX/FEI personal scanning electron microscope (PSEM) was used to perform all CCSEM analysis. Particle images from each sediment specimen were obtained using backscatter electron (BE) collection from an SEM operated in variable pressure mode. The chemical composition of individual particles was identified by energy dispersive x-ray spectroscopy (EDS) using an ASPEX/FEI OmegaMax™ silicon drift detector (SDD) with an ultra-thin window (permitting light element (Carbon and Oxygen) detection). Standard operating conditions for

the SEM consisted of an accelerating voltage of 25 keV, a beam current of approximately 1.0 nA, and a working distance of approximately 16 mm.

Individual particle data from each sediment sample was collected using an automated mode with both the electron beam and SEM stage being moved via computer control. The use of the automated image analysis mode required specific software set-up conditions be established prior to SEM analysis and data collection. The first was that the BE signal threshold was calibrated to separate the sediment particles (also referred to as “features” in the analysis) on the filter from the filter itself. The primary concern of this investigation was the inorganic particles in the various sediment samples which have an atomic number greater than carbon (atomic number 7). Thus, a binary threshold was programmed into the software so that the BE signal strength for each feature was greater than the carbon filter. Due to the possession of a low atomic number by carbon, the binary threshold for each feature was programmed with relative ease. The use of a detection limit above the aforementioned threshold allowed for automated analysis while the software was operating in search and detect mode. This meant that all inorganic particles adhered to the filter were subjected to detection and analysis during the automated feature analysis (AFA), and particle inclusion during the process was not constrained to features with a specific composition. Thus, the generation of particle subsets occurred. For instance, metal bearing particles within the sediment samples were recorded as an individual subset of the analyzed particles and could be subsequently isolated in the CCSEM data.

The capture of x-ray data at the SEM electron beam was accomplished using a programed analysis dwell time of a minimum of 10 seconds per particle and/or the acquisition of 10,000 X-ray counts. Image rasters were then compiled for any given inorganic particle or sample feature. Throughout this process, information in regards to the average composition of the whole particle was recorded and then stored. The identification of specific elements in the featured x-ray spectrum was accomplished with the use of the software vector editor. Thus, the semi-quantitative analysis of the elements in the spectrum was achieved. The determination of individual elements was the result of a vector calculation (filter-fit) by the software.

The standard spectra for the elements were used with the standards collected by the x-ray detector for the machine and resulted in the development of a technique which assumed that the unknown spectra could be represented as a weighted sum of the reference spectra. Within the weighted sum, the k-ratio remained a

constant and was closely related to the weight percentage. Additionally, a goal in the order of 4,500 features was strived for during each sediment sample analysis. Elements of interest included sodium (Na), magnesium (Mg), aluminum (Al), silicon (Si), phosphorus (P), sulfur (S), chlorine (Cl), potassium (K), calcium (Ca), titanium (Ti), chromium (Cr), manganese (Mn), iron (Fe), nickel (Ni), copper (Cu), and zinc (Zn).

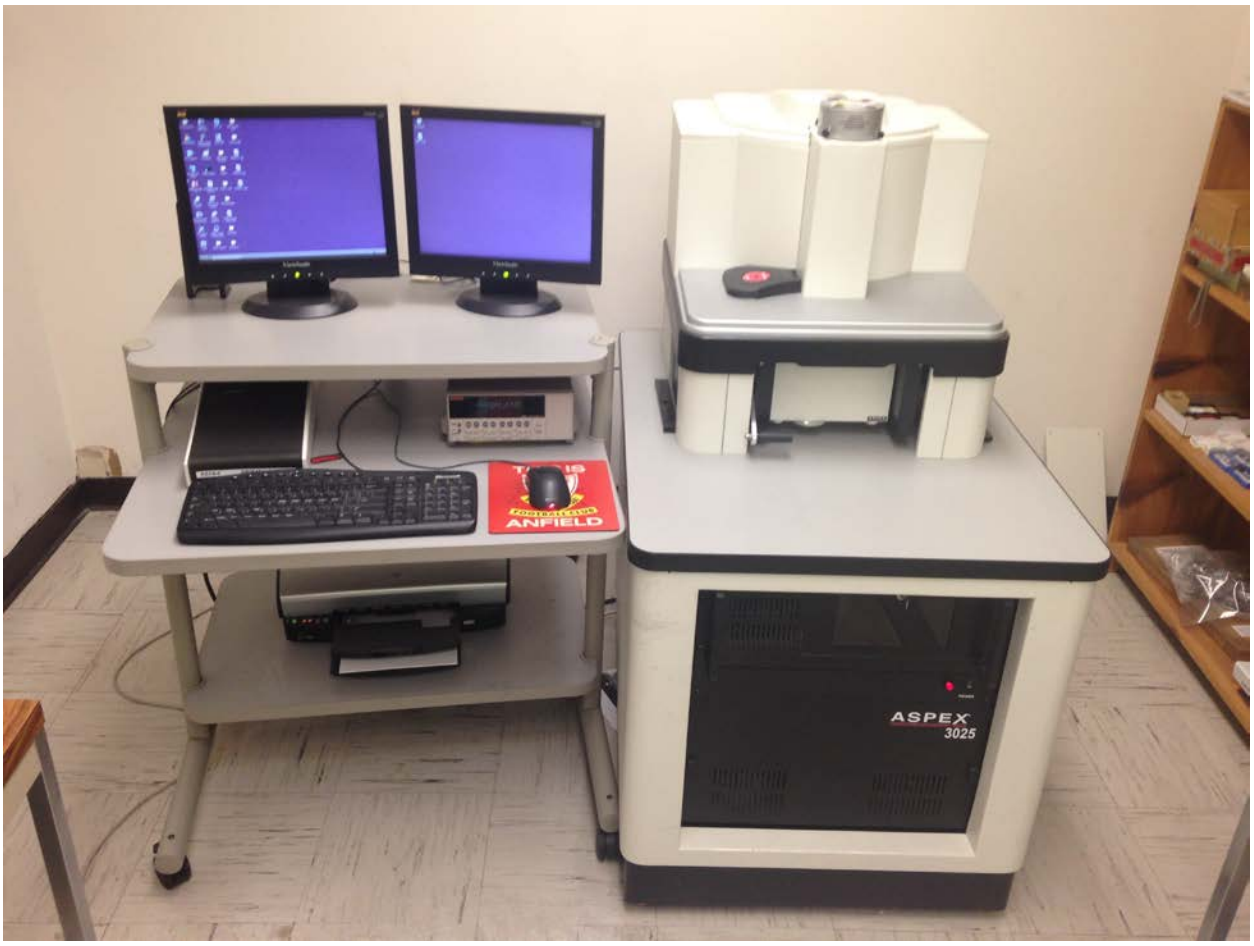

Figure 4-2 Computer Controlled Scanning Electron Microscope

Upon the identification of mineralogical constituents of a sample (in the CCSEM data), the comparison of constituents to those of the other sediment samples in the study was made by filtering the data through the linear classification system. Class numbers and the class rules used to develop the linear classification scheme are listed in Table 4-1. All data collected during this study was filtered through this linear classification scheme.

Table 4-1 Linear Classification System and Parameters

Class	Parameters
1	Si > 98%
2	Ca > 98%
3	Fe > 98%
4	Na > 98%
5	Al > 99%
6	Ti > 60%
7	Zn > 4%
8	SiAl > 98% and Si < 50%
9	SiAl > 98% and Si > 75%
10	AlSi > 98%
11	SCa > 98%
12	CaSi > 98%
13	FeS > 98% and S > 3%
14	Ca Mg > 98% and Ca > 3% and Mg > 3%
15	KCl > 98% and K > 3% and Cl > 3%
16	FeP > 98% and Fe > 60%
17	FeSi > 98%
18	MgSi > 98% and Mg > 3%
19	SiNa > 98%
20	NaCl > 98% and Cl > 3%
21	NaFe > 98%
22	FeCa > 98%
23	FePSi > 98% and Fe > 3% and P > 3% and Si > 3%
24	FeNaP > 98%
25	NaMgSi > 98% and Na > 3% and Mg > 3% and Si > 3%
26	NaAlFe > 98% and Na > 3% and Al > 3% and Fe > 3%
27	NaSiFe > 98% and Na > 3% and Si > 3% and Fe > 3%
28	NaSiCa > 98% and Na > 3% and Si > 3% and Ca > 3%
29	MgSiCa > 98% and Mg > 3% and Si > 3% and Ca > 3%
30	AlSiFe > 98% and Al > 3% and Si > 3% and Fe > 3%
31	AlSiK > 98% and Al > 3% and Si > 3% and K > 3%
32	AlSiCa > 98% and Al > 3% and Si > 3% and Ca > 3%
33	AlSiNa > 98% and Al > 3% and Si > 3% and Na > 3%
34	NaAlSiCa > 98% and Na > 3% and Al > 3% and Si > 3 % and Ca > 3%

Table 4-1 Continued

35	NaAlSiFe > 98% and Na > 3% and Al > 3% and Si > 3 % and Fe > 3%
36	NaAlSiK > 98% and Na > 3% and Al > 3% and Si > 3 % and K > 3%
37	AlSiKFe > 98%
38	AlSiFeMg > 98%
39	AlSiFeP > 98%
40	AlSiFeCa > 98% and Al > 3% and Si > 3% and Fe > 3% and Ca > 3%
41	AlSiKCa > 98% and Al > 3% and Si > 3% and K > 3% and Ca > 3%
42	MgAlSiCa > 98% and Mg> 3% and Al > 3% and Si > 3% and Ca > 3%
43	MgCaSiFe > 98% and Mg> 3% and Ca > 3% and Si > 3% and Fe > 3%
45	AlSiKFeCa > 98% and Al > 3% and Si > 3% and K > 3% and Fe > 3% and Ca > 3%
46	NaMgAlSiFe > 98% and Na > 3% and Mg > 3% and Al > 3% and Si > 3% and Fe > 3%
47	MgAlSiKFe > 98% and Mg > 3% and Al > 3% and Si > 3% and K > 3% and Fe > 3%
48	MgAlSiCaFe > 98% and Mg > 3% and Al > 3% and Si > 3% and Ca > 3% and Fe > 3%
49	NaAlSiCaFe > 98% and Na > 3% and Al > 3% and Si > 3% and Ca > 3% and Fe > 3%
50	FePSiAlNa > 98% and Fe > 3% and P > 3% and Si > 3% and Al > 3% and Na > 3%
51	NaAlSiKFe > 98% and Na > 3% and Al > 3% and Si > 3% and K > 3% and Fe > 3%
52	MgAlSiKFeCa > 98% and Mg > 3% and Al > 3% and Si > 3% and K > 3% and Fe > 3% and Ca > 3%
53	MgAlSiKFeNa > 98% and Mg > 3% and Al > 3% and Si > 3% and K > 3% and Fe > 3% and Na > 3%
54	MgAlSiCaFeNa > 98% and Mg > 3% and Al > 3% and Si > 3% and Ca > 3% and Fe > 3% and Na > 3%
55	MgAlSiKFeCa > 98% and Mg > 3% and Al > 3% and Si > 3% and K > 3% and Fe > 3% and Ca > 3%
56	NaAlSiKFeCaMg > 98% and Na > 3% and Al > 3% and Si > 3% and K > 3% and Fe > 3% and Ca > 3% and Mg > 3%
57	Ti > 3% and < 60%
58	Mn > 4%
100	Non-classified

Chapter 5

Results

A total of 16 soil and laterite samples from the Burkina Faso and Niger regions were analyzed. Upon completion of the experiment, the results were tabulated based upon the categorization of how the particles were sorted by the linear classification scheme in Table 4-1. An average of approximately 5,150 particles were analyzed per sample with a minimum of 2,061 particles analyzed in Burkina Soil 10A, and a maximum of 7,856 particles analyzed in Burkina Soil 12A in all 77,398 particles were analyzed.

Multiple approaches were taken in regards to data analysis. To begin with, average concentrations for each class were calculated for each of the 16 samples analyzed in an attempt to determine if there was a trend which could be identified in the Burkina Faso and Niger sediment samples. Upon the determination of the aforementioned average concentration for each class, a 1 % cut-off concentration was applied to restrict particle classes to 22 down from the original 60 classes. Table 5-1 summarizes the classes for the Burkina Faso and Niger sediment samples after applying the 1% cut-off, and the summary of the results for the 22 classes can be found in a table located in Appendix A.

After the data was analyzed and patterns were determined within particle classes, visual evaluations of the particles within the classes were conducted. SEM field of view (FOV), containing several particles, was examined and particles were examined at high magnification with the X-ray spectrum of each was collected at that time. Unique visual characteristics were identified which were associated with not only particular particle classes but also differentiated between soils and laterites.

Class	Parameters
1	Si > 98%
3	Fe > 98%
6	Ti > 60%
8	SiAl > 98% and Si < 50%
9	SiAl > 98% and Si > 75%
17	FeSi > 98%
30	AlSiFe > 98% and Al > 3% and Si > 3% and Fe > 3%
31	AlSiK > 98% and Al > 3% and Si > 3% and K > 3%
33	AlSiNa > 98% and Al > 3% and Si > 3% and Na > 3%
34	NaAlSiCa > 98% and Na > 3% and Al > 3% and Si > 3 % and Ca > 3%
35	NaAlSiFe > 98% and Na > 3% and Al > 3% and Si > 3 % and Fe > 3%
36	NaAlSiK > 98% and Na > 3% and Al > 3% and Si > 3 % and K > 3%
37	AlSiKFe > 98%
38	AlSiFeMg > 98%
39	AlSiFeP > 98%
40	AlSiFeCa > 98% and Al > 3% and Si > 3% and Fe > 3% and Ca > 3%
47	MgAlSiKFe > 98% and Mg > 3% and Al > 3% and Si > 3% and K > 3% and Fe > 3%
49	NaAlSiCaFe > 98% and Na > 3% and Al > 3% and Si > 3% and Ca > 3% and Fe > 3%
51	NaAlSiKFe > 98% and Na > 3% and Al > 3% and Si > 3% and K > 3% and Fe > 3%
56	NaAlSiKFeCaMg > 98% and Na > 3% and Al > 3% and Si > 3% and K > 3% and Fe > 3% and Ca > 3% and Mg > 3%
57	Ti > 3% and < 60%
58	Mn > 4%
100	Non-classified

Table 5-1: Relevant Classes to the Burkina Faso and Niger Regions

The data set indicated that the primary elements which comprised the Burkina Faso and Niger sediment samples were Al, Si, and Fe in varying proportions. Additionally, all samples with the exception of Burkina Soil 11A, Burkina Laterites 0, 3, 4 and 9 possessed particles above the cutoff for class 57 or Ti equal to 3- 60%. Comparisons of each class proportion relative to other soils or laterites were made with the use of a bar graph and may be viewed in appendix B. Overall, the majority of particles analyzed fell in class 30 otherwise known as the Al-Si-Fe class. Burkina soil samples particle percentages ranged from 43.6 – 58.1% whereas Burkina laterite particle percentages ranged from 56.0 – 90.8%. Also, the soil samples appeared to possess higher concentrations of classes 8 and 9 than the laterite samples with a combined total ranging from approximately 5.6% to 26.1% as compared to laterite ranges of approximately 2.0% to 14.6%. Soil samples possessed particles within single element classes of Si, Fe, and Si-Fe (classes 1, 3, and 17), however laterite samples, for the most part, did not.

Other notable classes included classes 31, 33, 34, 35, 36, 37, 38, 39, 40, 47, 49, and 51. Al-Si appear in the aforementioned classes with varying concentrations of Ca, Fe, Mg, Na, and K. Regardless of the combination of the elements, each constituents must compose at least three percent of the particle class. Classes 57, 58, and 100 are classes focused on capturing particles which were the outliers with class 57 particle having criteria of concentrations of between 3 - 60% Ti, class 58 having any concentration of Mn greater than 4%, and class 100 for particles that do not adhere to the criteria of the established linear classification scheme. Class 100, or otherwise unclassified particles, ranged from less than 1% to 6.1% and mainly present in the soil samples.

Ternary plots of class 30, or modal compositions of Al-Si-Fe, were graphed for all Burkina Soil and Laterite samples. Upon reviewing these plots, it was noted that Burkina Laterite samples exhibited a more linear trend comprised mainly of Al and Fe with diminishing quantities of Si of 35% or less. Highly matured laterites exhibited modal compositions dominated by greater 50% for particles within class 30. However, Burkina soil ternary plots exhibited less of a linear trend with higher ratios of Si content and a more erratic pattern between the soils samples themselves whereas the laterites tended to mimic each other's pattern.

Visual inspection via SEM FOV was completed for both soil and laterite particles within classes 1, 3, 8, 9, 30, 31, 37, and 100. Inspection revealed somewhat unique trends in particle characteristics associated with both particular classes and sediment samples. To begin with class 1 or Si-only particles (quartz) seen in soils (Figure

5-1) were less weathered and more angular in nature than class 1 particles seen in laterites (Figure 5-2). Class 3 particles were, for the most part, visually relatively similar between soils and laterites (Figure 5-3 and 5-4), however certain soils possessed certain particles, which exhibited exceptional cubic habits and crystal intergrowth (5-5 and 5-6). Visually class 8 and 9 particles within soils mimicked the appearance of class one particles and possessed relatively low percentages of Al with drastic amounts of Si (Figure 5-7) whereas class 8 and 9 particles within laterites appeared much more fragmented and possessed relatively balanced amounts of Al and Si (Figure 5-8). Class 30 or Al-Si-Fe particles exhibited the greatest contrast in visual appearance between soils and laterites. In soils, class 30 particles appear as particles with relatively low levels of accreted Fe (Figure 5-9), but in laterites particles appear more rounded with accreted Fe in higher proportions (Figure 5-10). Al-Si-K or class 31 particles (Figures 5-11 and 5-12) again demonstrated the common trend of more weathered particles present in laterites versus their more angular counterparts present in soils. Additionally, the elemental composition varied in regards to proportions. Soil particles were dominated by higher percentages of silicon whereas laterite particles possessed relatively equal proportions of aluminum and silicon with somewhat reduced quantities of potassium. Al-Si-K-Fe or class 37 particles (Figure 5-13 and 5-14) somewhat differed in appearance in that particles from the soils appeared to be less weathered relative to particles seen in laterites, but the elemental compositions and proportions were very similar in nature as a whole. Non-classified or class 100 minerals (Figures 5-15 through 5-18) varied greatly in composition and appearance for both soils and laterites. However, as a general rule these minerals appeared to be highly angular in nature and possessed accreted minerals on an Al-Si particle with exception to a few particles seen in the laterites. A small amount of the particles within class 100 were sulfates (Figure 5-17) or variations of Fe like the Cr-Fe particle in figure 5-18.

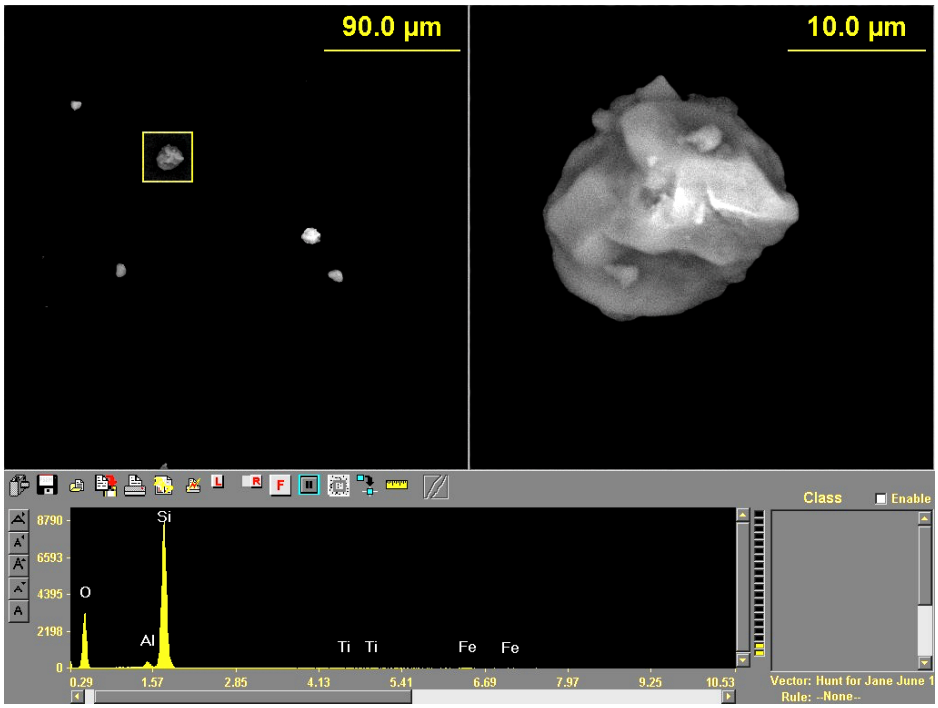

Figure 5-1: Example of a class 1 or Si particle from Burkina Soil 6A.

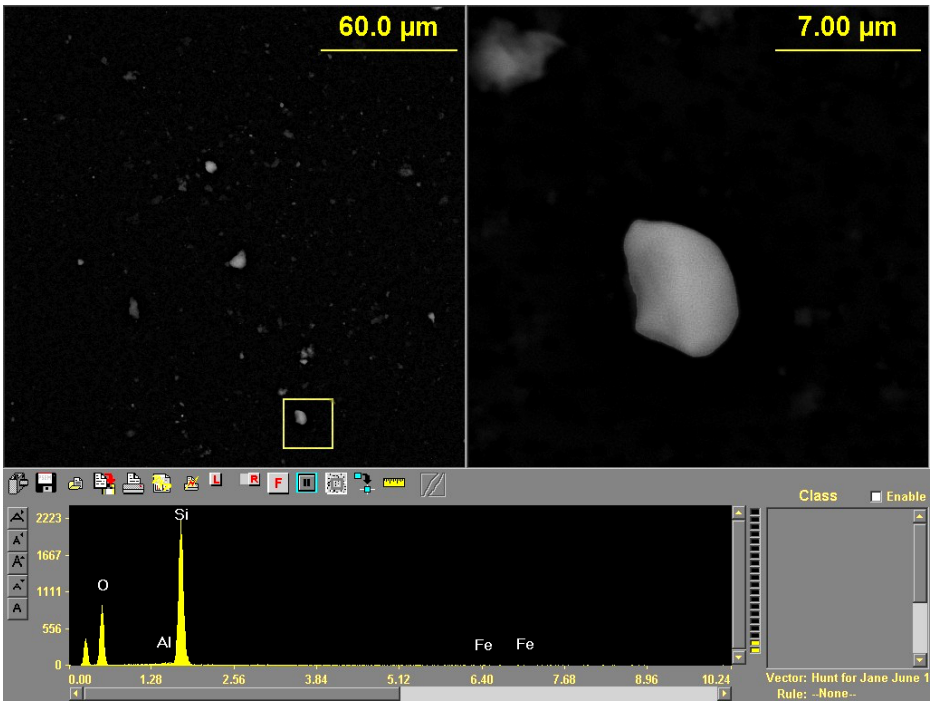

Figure 5-2: Example of a typical class 1 or Si particle from Burkina Laterite 3.

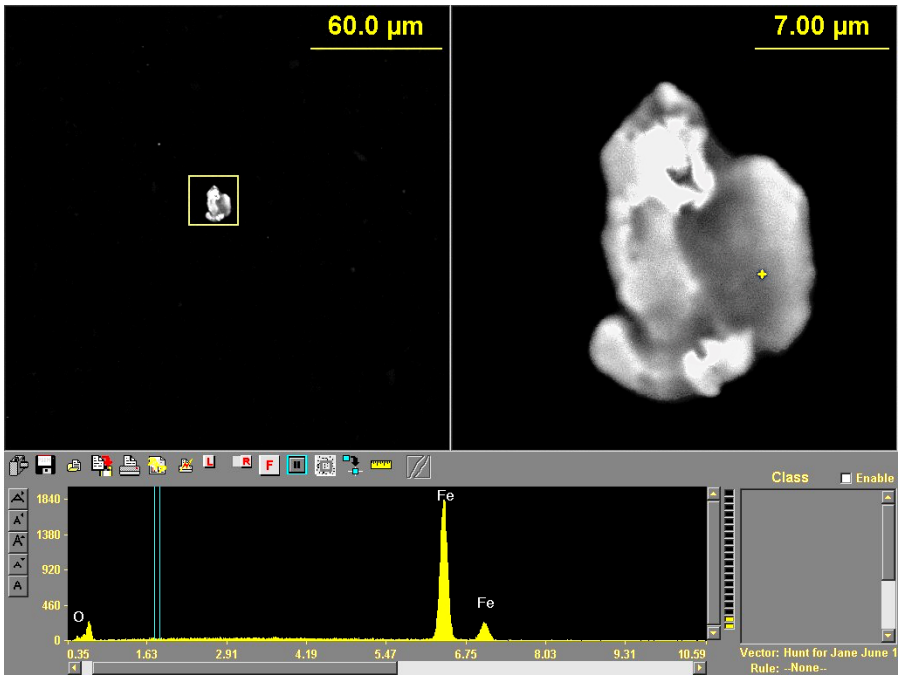

Figure 5-3: An example of a class 3 or Fe particle from Burkina Soil 6A.

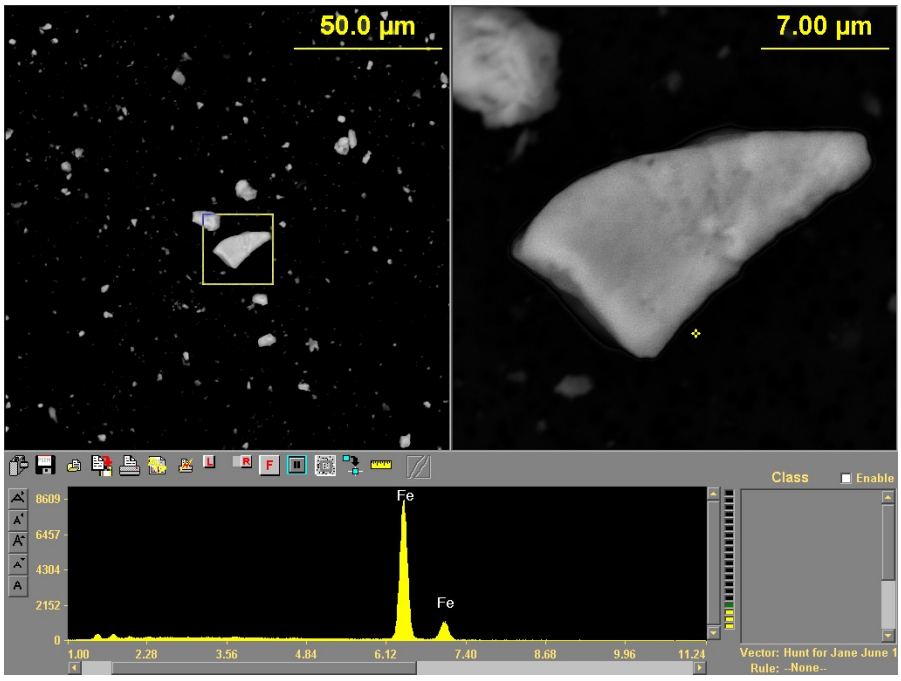

Figure 5-4: An example of a class 3 or Fe particle from Burkina Laterite 0.

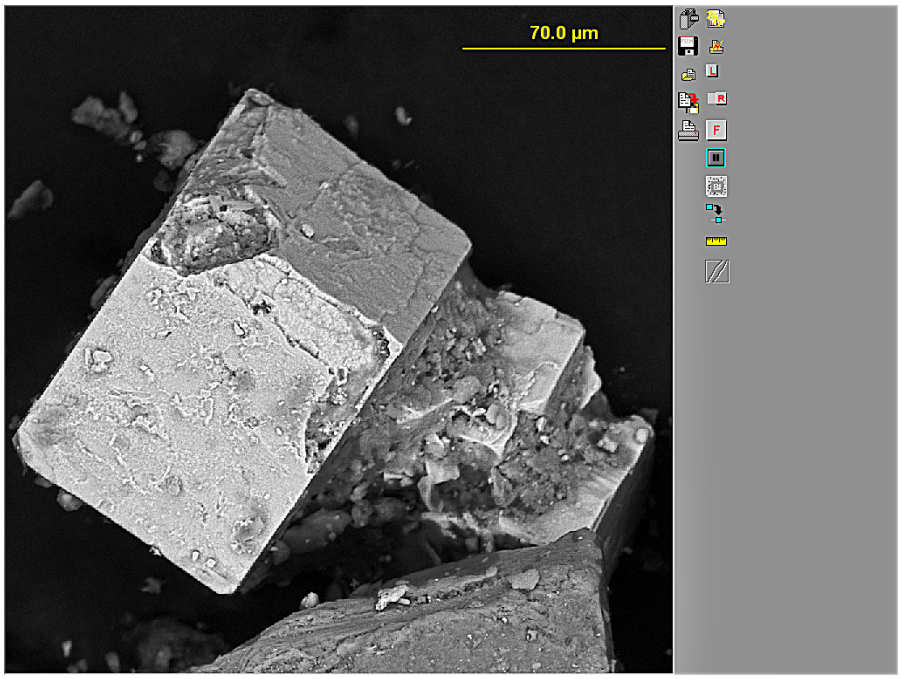

Figure 5-5: An example of a class 3 or Fe particle exhibiting cubic crystal form from Burkina Soil 11A.

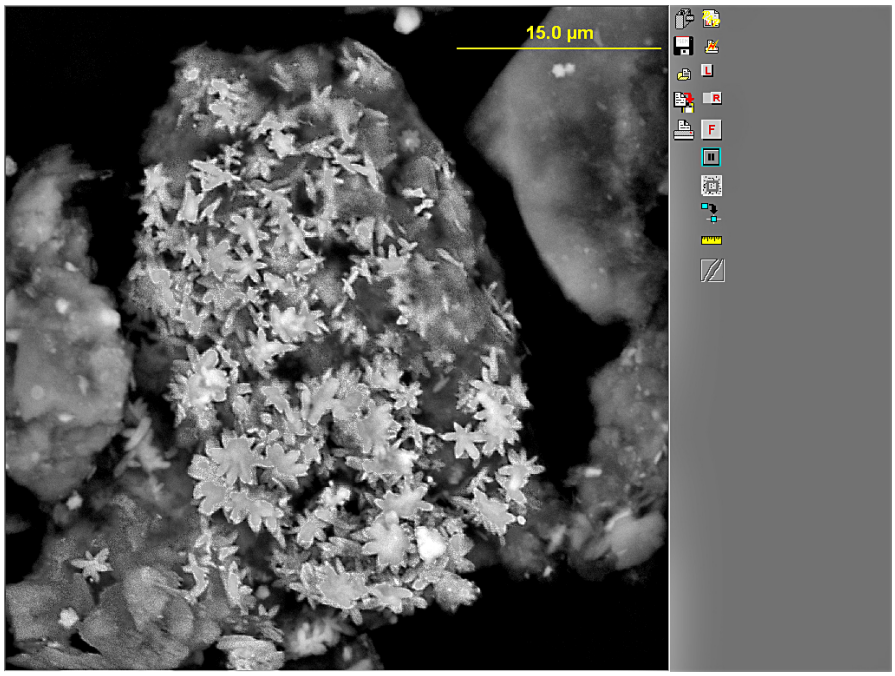

Figure 5-6: Class 3 or Fe particles exhibiting intergrown crystals from Burkina Soil 11A.

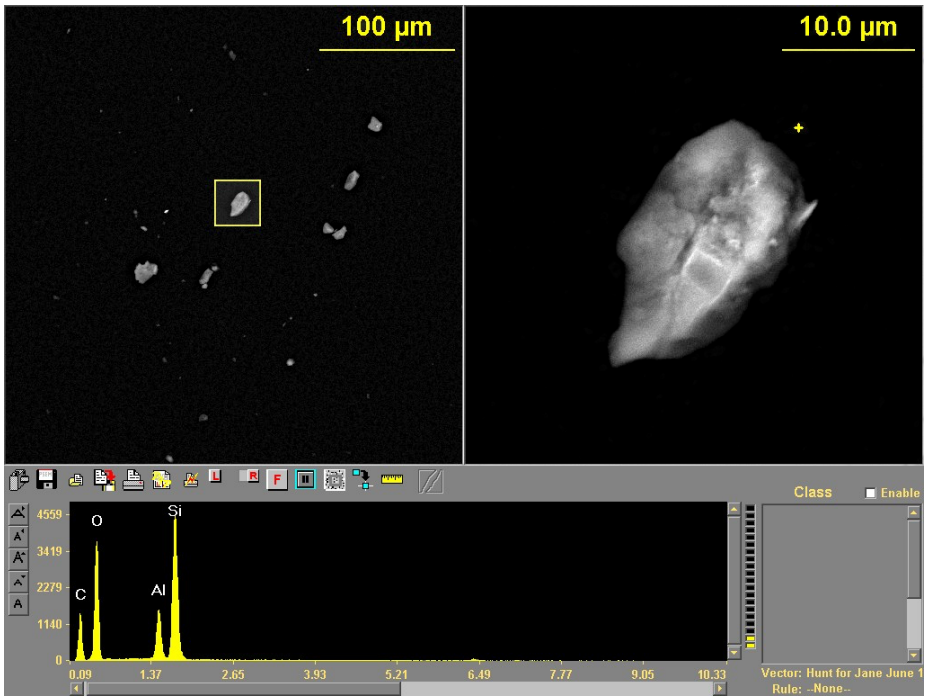

Figure 5-7: An example of a class 9 or Al-Si particle from Burkina Soil 6A.

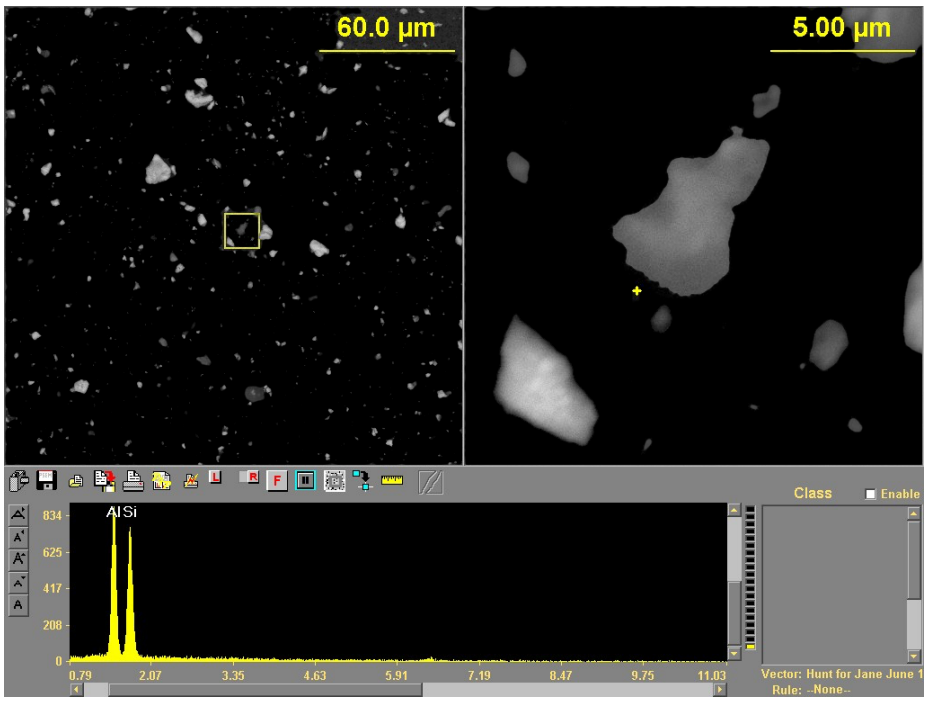

Figure 5-8: An example of a class 9 or Al-Si particle from Burkina Laterite 0.

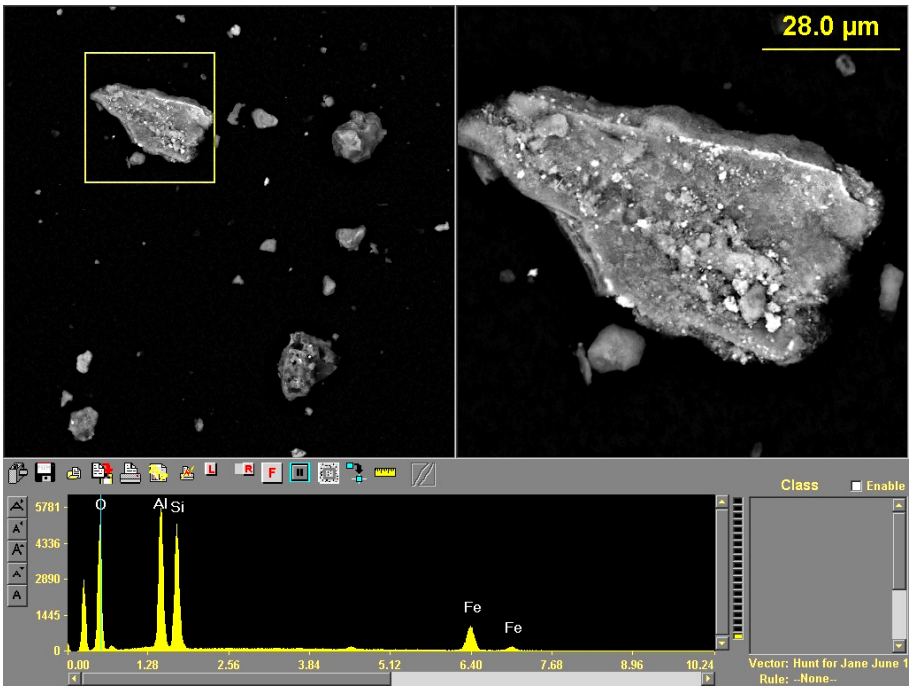

Figure 5-9: An example of a class 30 or Al-Si-Fe particle from Burkina Soil 10A.

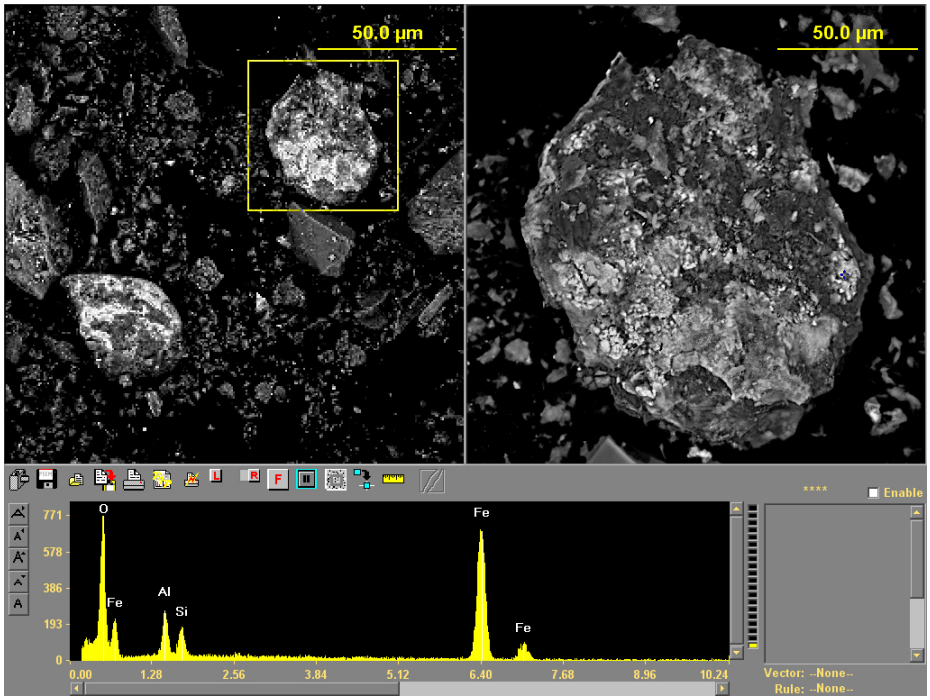

Figure 5-10: An example of a class 30 or Al-Si-Fe particle from Burkina Laterite 8.

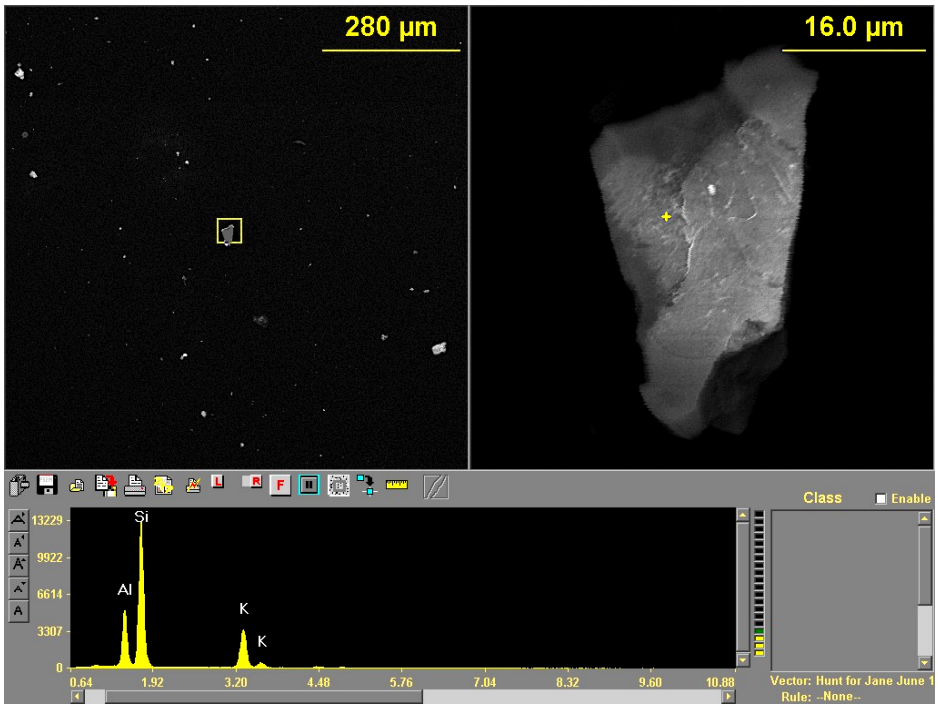

Figure 5-11: An example of a class 31 or Al-Si-K particle from Burkina Soil 7A.

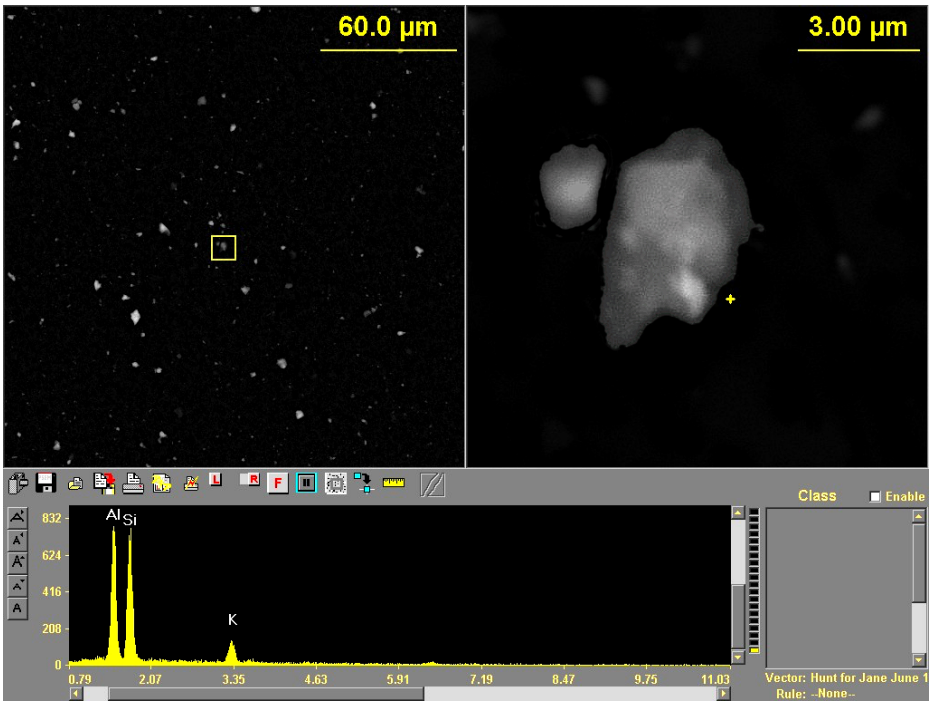

Figure 5-12: An example of a class 30 or Al-Si-K particle from Burkina Laterite 0.

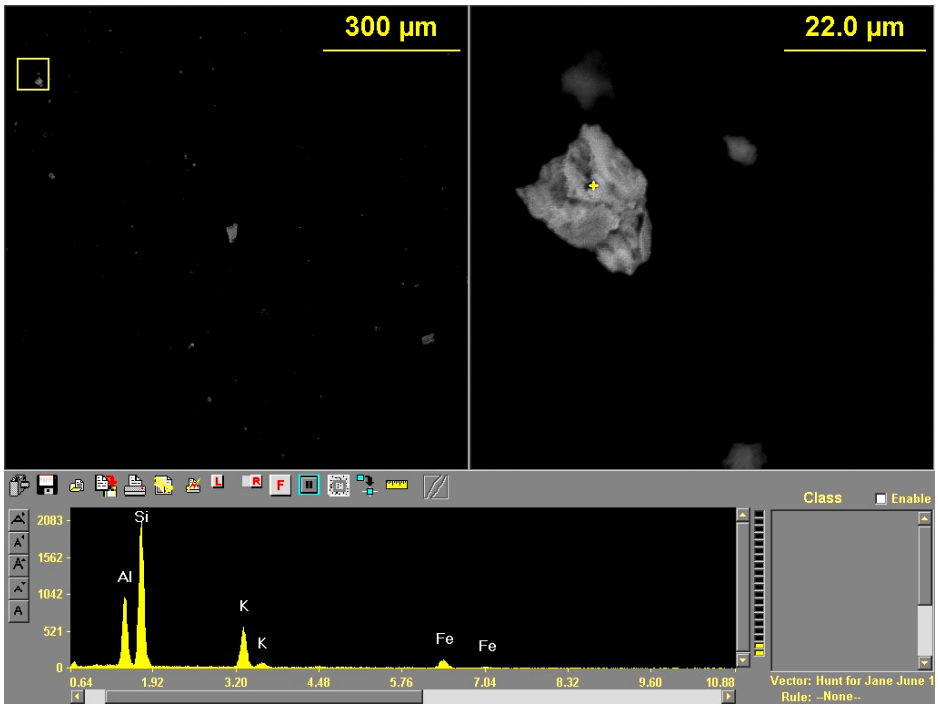

Figure 5-13: An example of a class 37 or Al-Si-K-Fe particle from Burkina Soil 7A.

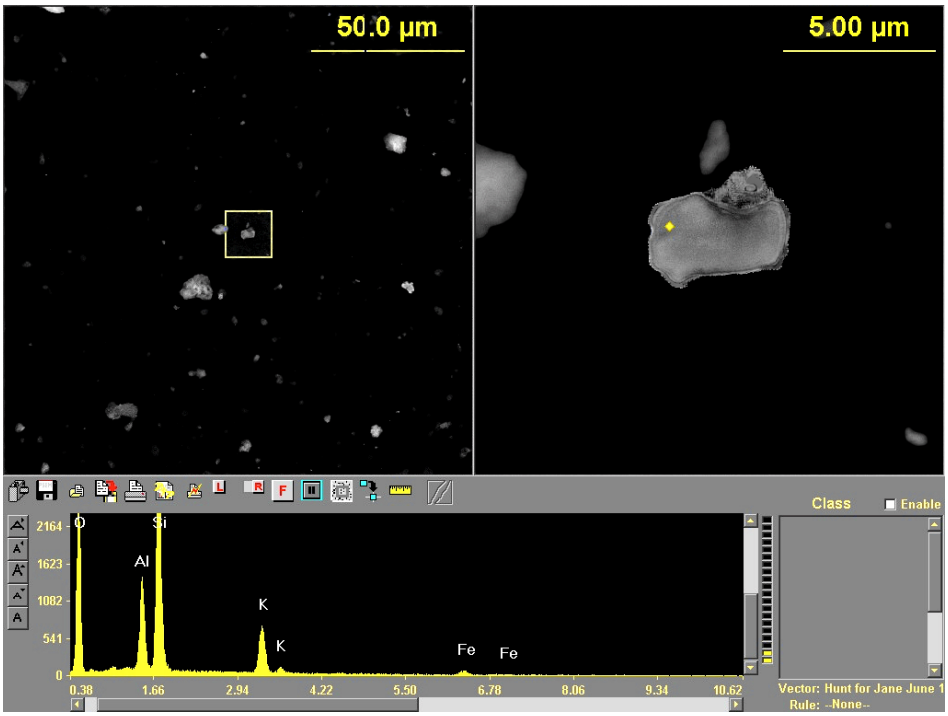

Figure 5-14: An example of a class 37 or Al-Si-K-Fe particle from Burkina Laterite 3.

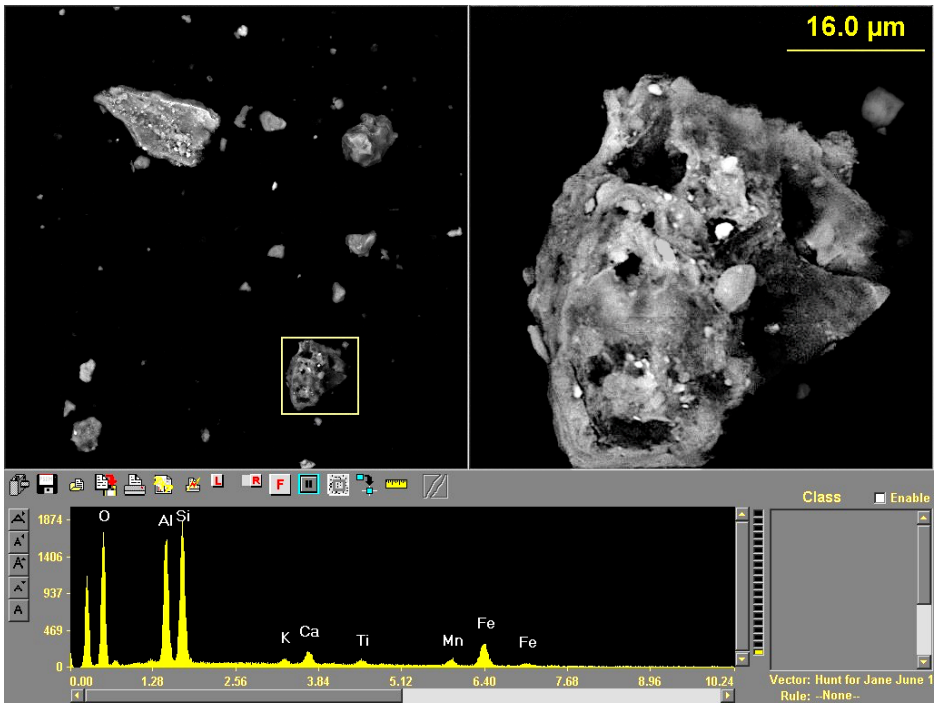

Figure 5-15: An example of a class 100 or non-classified particle from Burkina Soil 10A.

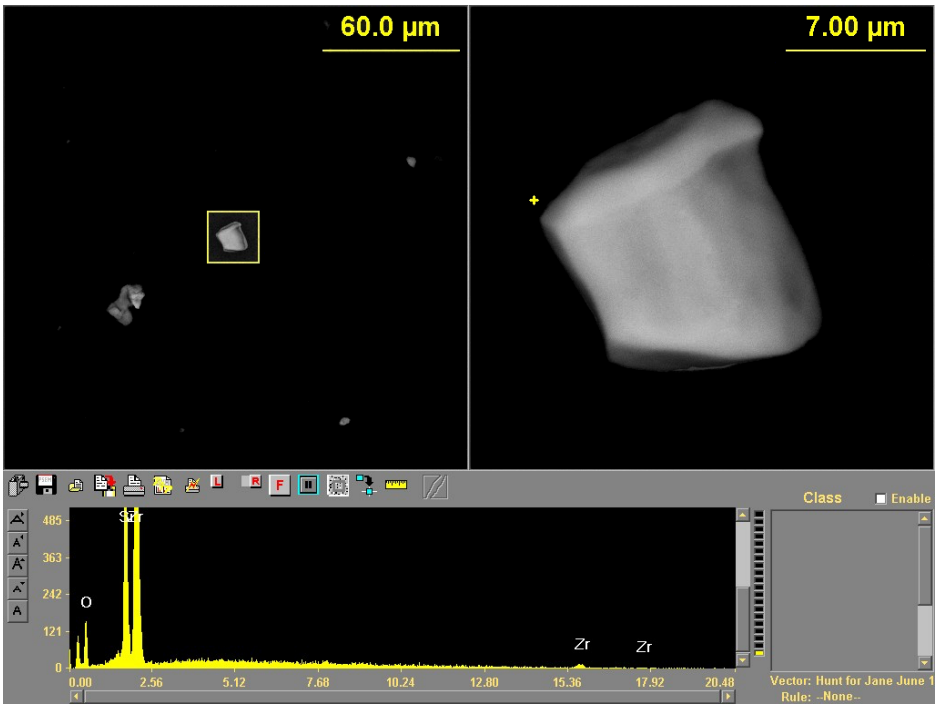

Figure 5-16: An example of a class 100 or non-classified particle from Burkina Soil 6A.

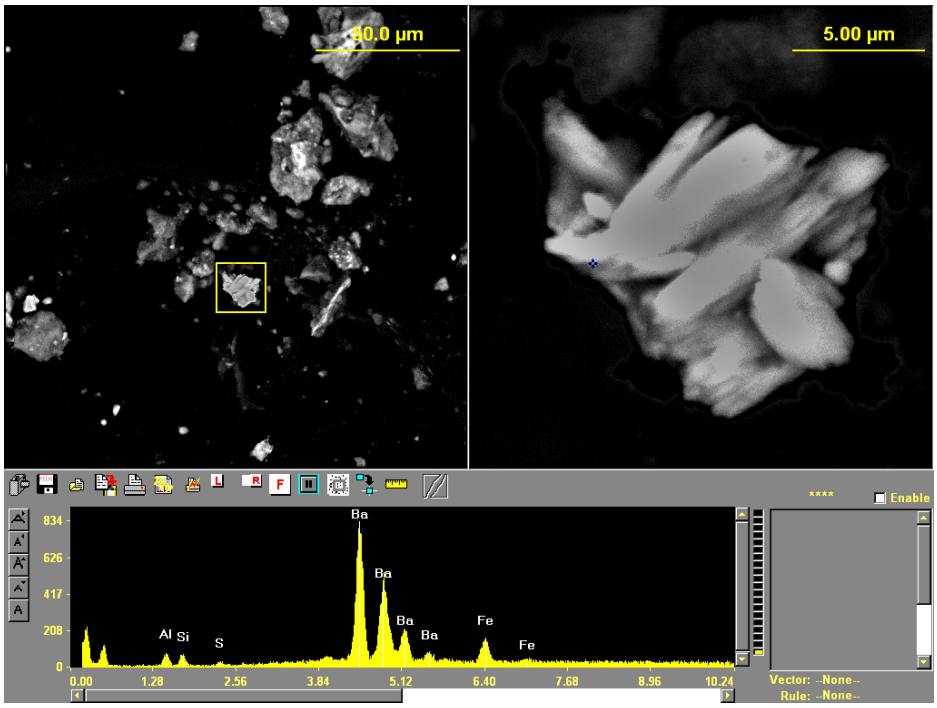

Figure 5-17: An example of a class 100 or non-classified particle from Burkina Laterite 3.

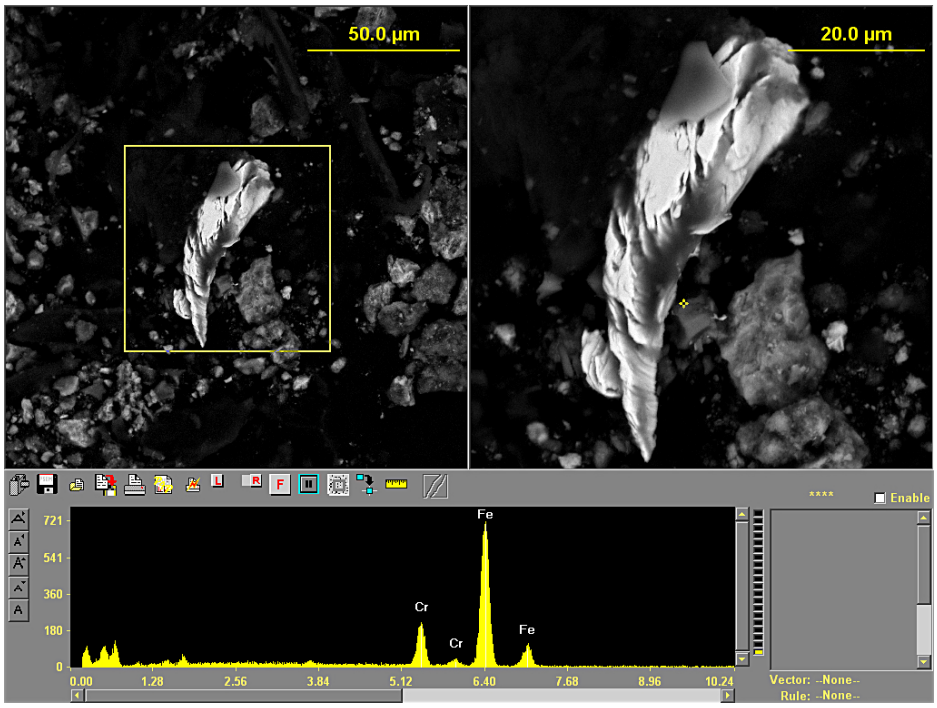

Figure 5-18: An example of a class 100 or non-classified particle from Burkina Laterite 4.

Burkina Soil 4A

Burkina Soil 4A was mainly comprised of the following classes: 1, 3, 8, 9, 30, 31, 37, 57, and 100. The majority of the particles, approximately 48.7%, were class 30 or Al-Si-Fe particles. Although, 48.7% is towards the lower range of ratio of 43 – 58% class 30 particles relative to the total particles analyzed, the aforementioned percentage was consistent with the other soils analyzed. Additionally, figure 5-19 illustrates the trending of particles within class 30 and demonstrates that majority particles consisted of less than 25% Fe, approximately 45% Al, and 30% Si. The next largest grouping of particles were the class 8 and 9 or Al-Si particles comprising approximately 26.1% of the total particles analyzed. The last dominate class was 37 or Al-Si-K-Fe particles with approximately 5.9%. Additionally, Burkina Soil 4A possessed a moderate portion of class 1 or Si minerals at 2.3%. The presence of the Si class is a unique characteristic of the Burkina Soils whereas Burkina Laterites are almost devoid of any Si rich minerals.

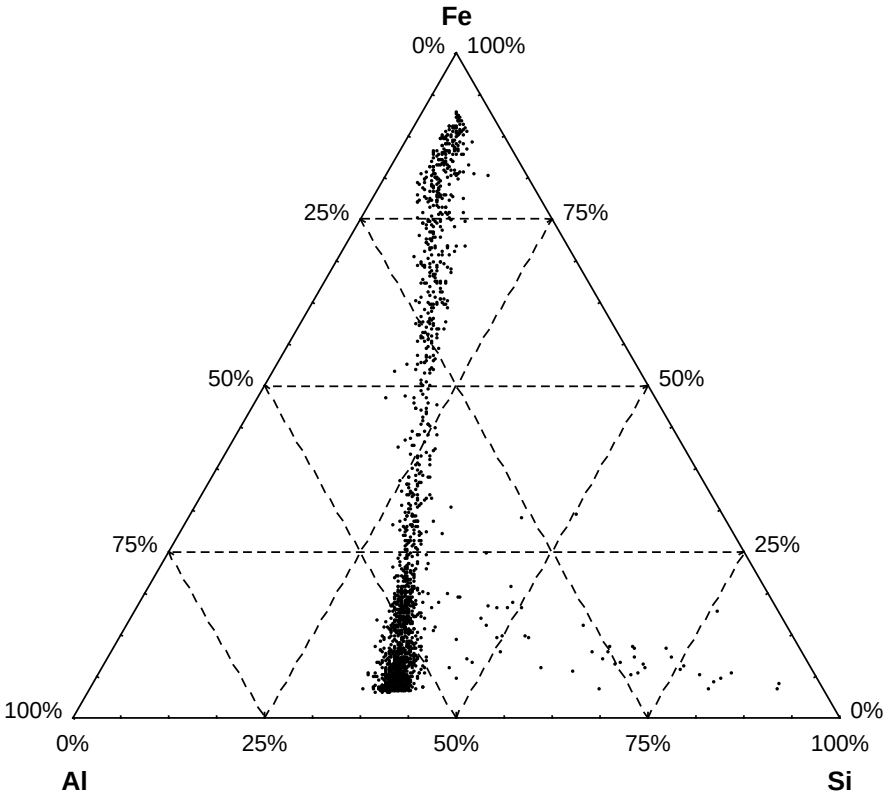

Figure 5-19: Ternary graph of Al, Si, and Fe for Class 30 particles within Burkina Soil 4A. The total number of particles plotted was 1,578 of the 3,240 particles analyzed.

Burkina Soil 5A

Burkina Soil 5A was comprised of the following classes: 1, 3, 8, 9, 30, 31, 35, 37, 38, 47, 51, 57, and 100. Approximately 51.2% of the particles analyzed were class 30 or Al-Si-Fe particle which was well within the range of 43 – 58% class 30 particles seen in the other soils. Figure 5-20 illustrates that particles within class 30 possessed a slightly higher ratio of Fe; however the majority of particles consisted of less than 50%. The next largest grouping of particles was class 37 comprising approximately 7.3% of the total particles analyzed. A close third was class 1 with approximately 5.9% which was the third highest silica or quartz percentage seen in all samples analyzed.

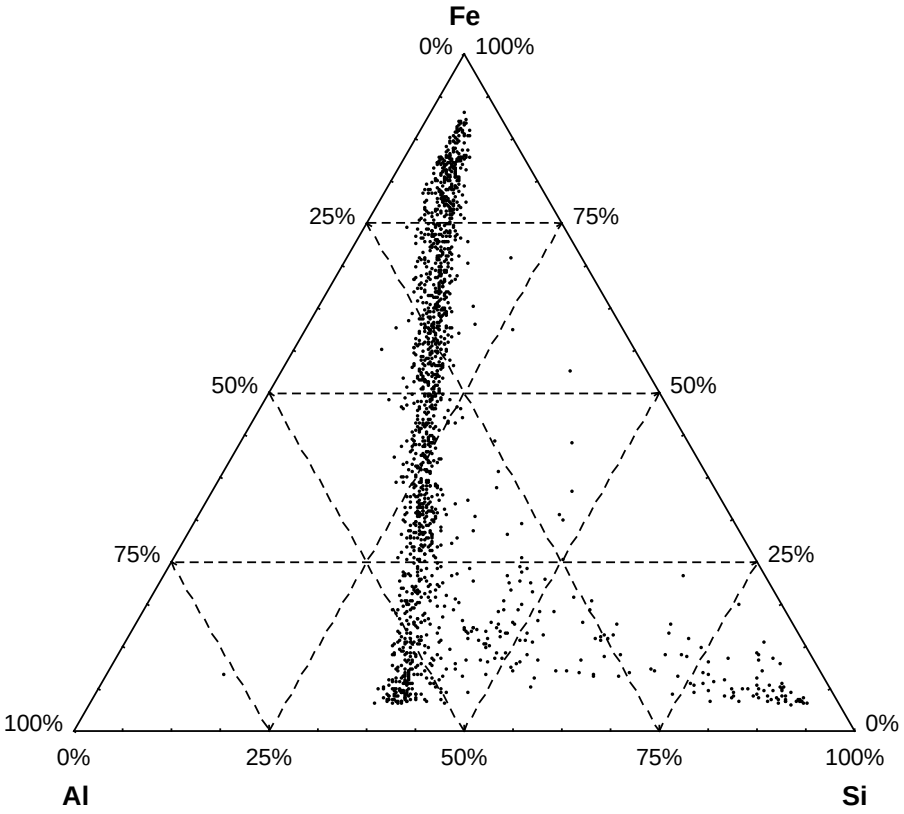

Figure 5-20: Ternary graph of Al, Si, and Fe for Class 30 particles within Burkina Soil 5A. The total number of particles plotted was 1,497 of the 2,925 particles analyzed.

Burkina Soil 6A

Burkina Soil 6A was mostly comprised of the following classes: 1, 8, 9, 30, 31, 35, 36, 37, 49, and 57. Approximately 43.6% of the particles analyzed were class 30 or Al-Si-Fe particle which was the lowest percentage of class 30 for all samples analyzed. Figure 5-21 illustrates a more representative trend of particles within class 30 for the soils. As seen in Burkina Soil 4A, the majority of particles consisted of less than 25% Fe, approximately 45-55% Al, and roughly 30% Si. The next largest groupings of particles were classes 8 and 9 comprising approximately 17.3% of the total particles analyzed. Burkina Soil 6A also possessed the highest percentage of class 57 or Ti particles of all samples analyzed.

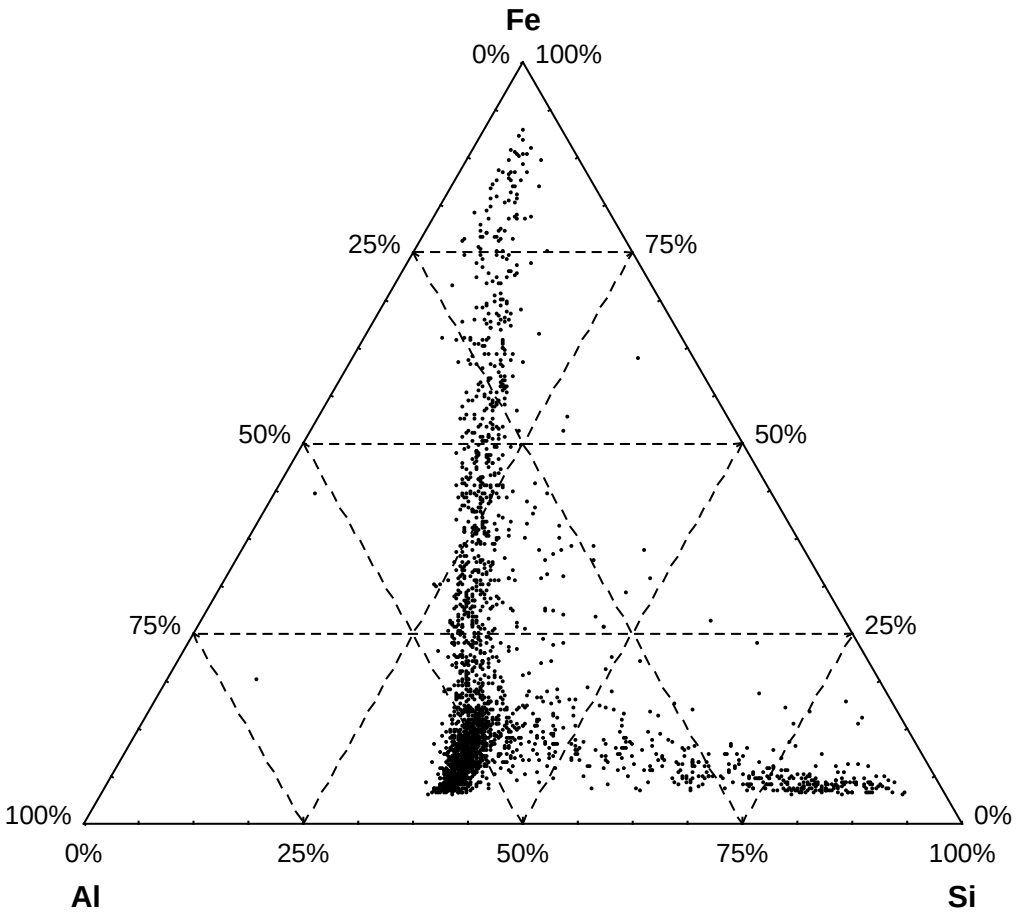

Figure 5-21: Ternary graph of Al, Si, and Fe for Class 30 particles within Burkina Soil 6A. The total number of particles plotted was 2,263 of the 5,194 particles analyzed.

Burkina Soil 7A

Burkina Soil 7A was comprised of the following 15 classes making it the most diverse in classes of all samples analyzed: 1, 3, 8, 9, 17, 30, 31, 33, 35, 37, 47, 51, 57, 58, and 100. Approximately 43.6% of the particles analyzed were class 30 or Al-Si-Fe particle which tied Burkina Soil 6A in having the lowest percentage of class 30 for all samples analyzed. Figure 5-22 illustrates a more representative trend of particles within class 30 for the soils; although the particles plotted did appear to be more segregated and demonstrated less of a gradient transition towards the Fe rich particles. The majority of the particles were composed of less than 25% Fe, approximately 45-55% Al, and roughly 30% Si. After class 30, classes 35 and 37 contributed approximately 6-7% of total particles analyzed; these classes are comprised of Al-Si-Fe particles with either the addition of Na or K.

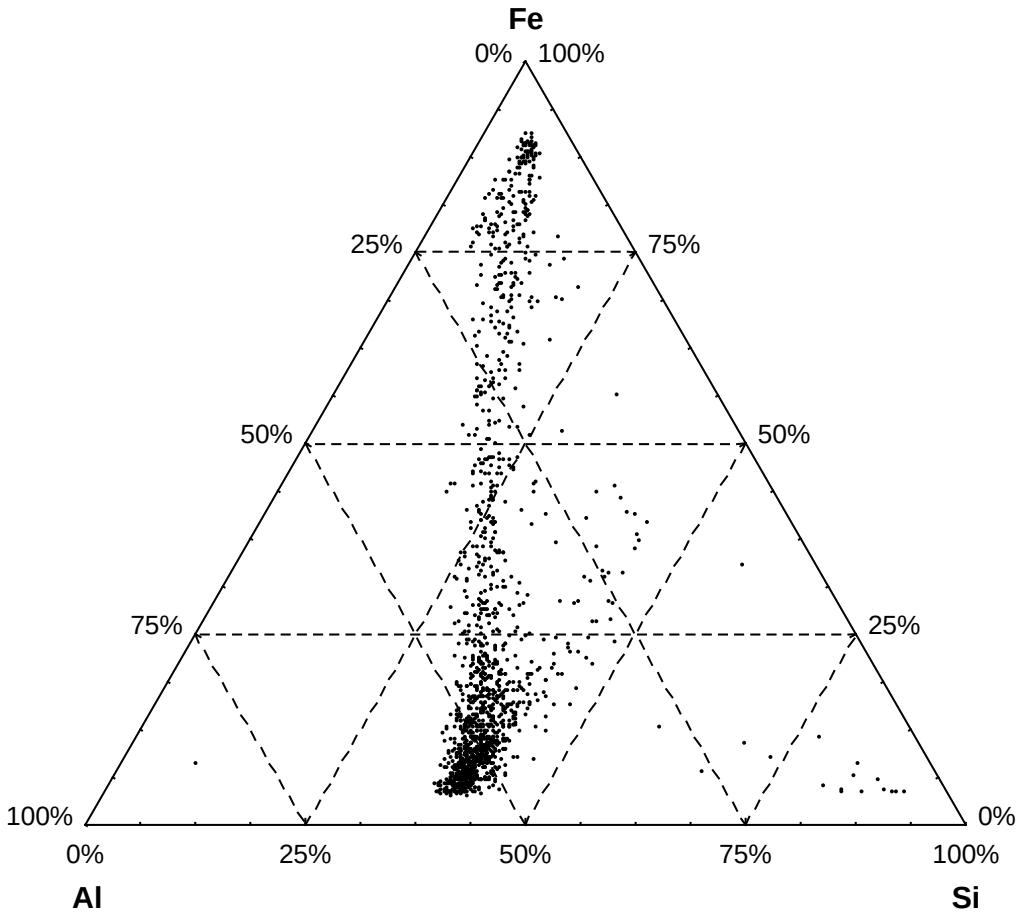

Figure 5-22: Ternary graph of Al, Si, and Fe for Class 30 particles within Burkina Soil 7A. The total number of particles plotted was 1,364 of the 3,132 particles analyzed.

Burkina Soil 10A

Burkina Soil 10A was comprised of the following classes: 1, 8, 9, 30, 31, 35, 36, 37, 47, 49, 51, 57, 58, and 100. Of the particles analyzed, approximately 51.4% were class 30 or Al-Si-Fe particle. Figure 5-23 illustrates a more linear trend of particles within class 30 than was seen in the other soils. In fact, the trending of particles appears to be somewhat in between what is seen in the soils and laterites analyzed. The majority of the particles were composed of greater than 50% Fe. Burkina Soil 10A also possessed the highest percentage of class 35 or Na-Al-Si-Fe particles at 14.3% which was two to three times higher than the other soils. Classes 8 and 9 accounted for approximately 9.6% of the total particles analyzed.

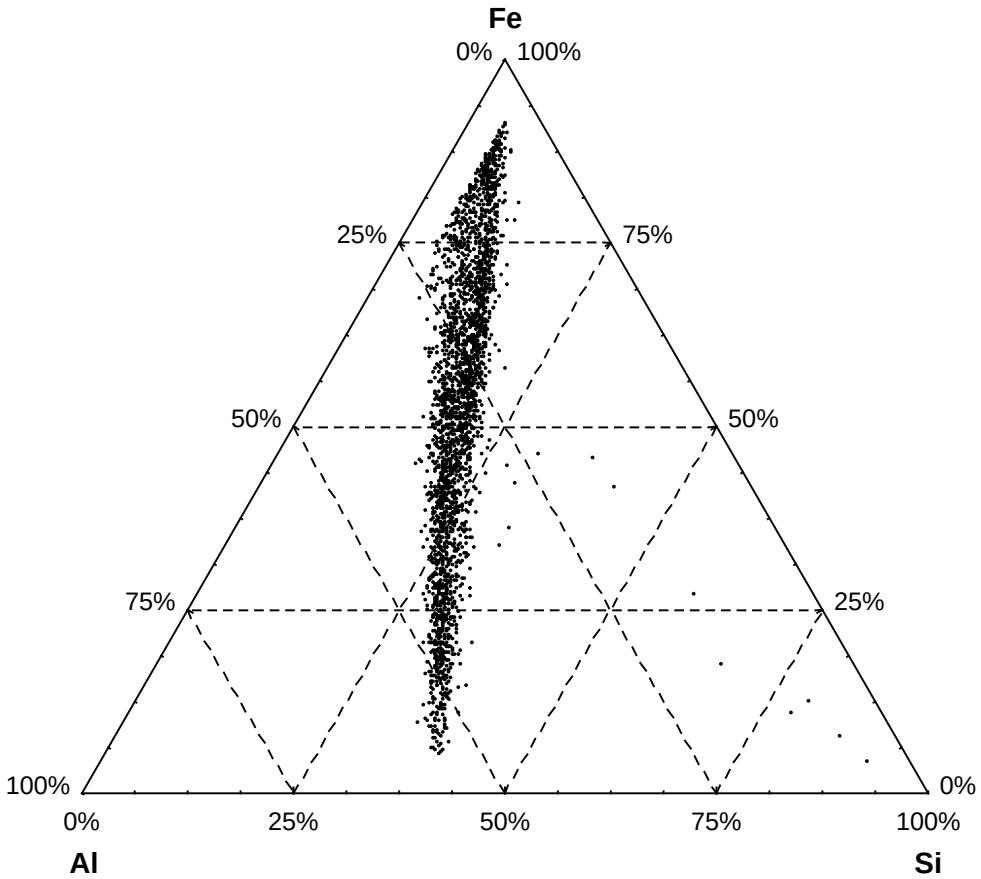

Figure 5-23: Ternary graph of Al, Si, and Fe for Class 30 particles within Burkina Soil 10A. The total number of particles plotted was 1,061 of the 2,061 particles analyzed.

Burkina Soil 11A

Burkina Soil 11A was mainly comprised of the following classes: 1, 3, 6, 8, 9, 30, 35, 37, 38, 39, 47, 51, and 100. Of the particles analyzed, approximately 58.1% were class 30 or Al-Si-Fe particle which was the highest percentage of all soils analyzed. Figure 5-24 illustrates somewhat typical trending of particles within class 30 for the Burkina soils. The majority of the particles were composed of less than 50% Fe. Burkina Soil 10A also possessed the highest percentage of class 37 or Al-Si-K-Fe particles at 11.4%. Classes 8 and 9 only accounted for approximately 5.6% of the total particles analyzed. Additionally, Burkina Soil 11A possessed the highest percentage of class 3 or Fe particles with 2.9% and was the only soil analyzed to possess a significant proportion of class 6 or Ti rich particles.

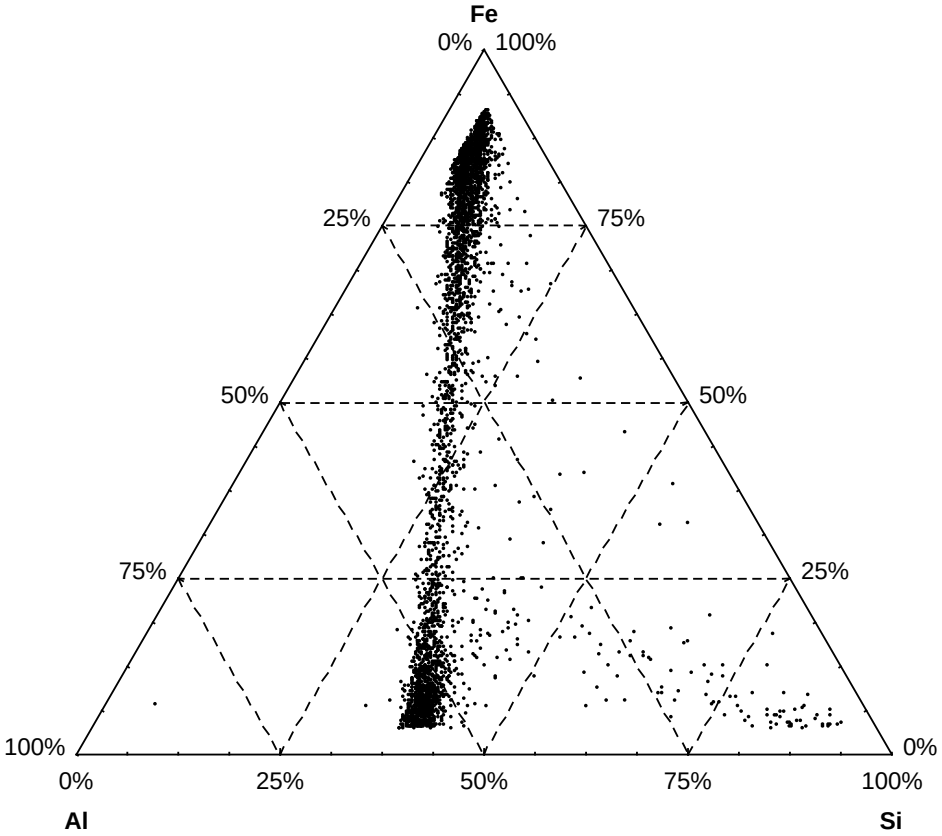

Figure 5-24: Ternary graph of Al, Si, and Fe for Class 30 particles within Burkina Soil 11A. The total number of particles plotted was 3,349 of the 5,767 particles analyzed.

Burkina Soil 12A

Burkina Soil 12A was comprised of the following classes: 1, 3, 6, 8, 9, 30, 35, 37, 38, 39, 47, 51, and 100. Of the particles analyzed, approximately 58.1% were class 30 or Al-Si-Fe particle which was the highest percentage of all soils analyzed. Figure 5-25 illustrates somewhat typical trending of particles within class 30 for the Burkina soils. The majority of the particles were composed of less than 50% Fe. Burkina Soil 10A also possessed the highest percentage of class 37 or Al-Si-K-Fe particles at 11.4%. Classes 8 and 9 only accounted for approximately 5.6% of the total particles analyzed. Additionally, Burkina Soil 12A possessed the highest percentage of class 3 or Fe particles with 2.9% and was the only soil analyzed to possess a significant proportion of class 6 or Ti rich particles.

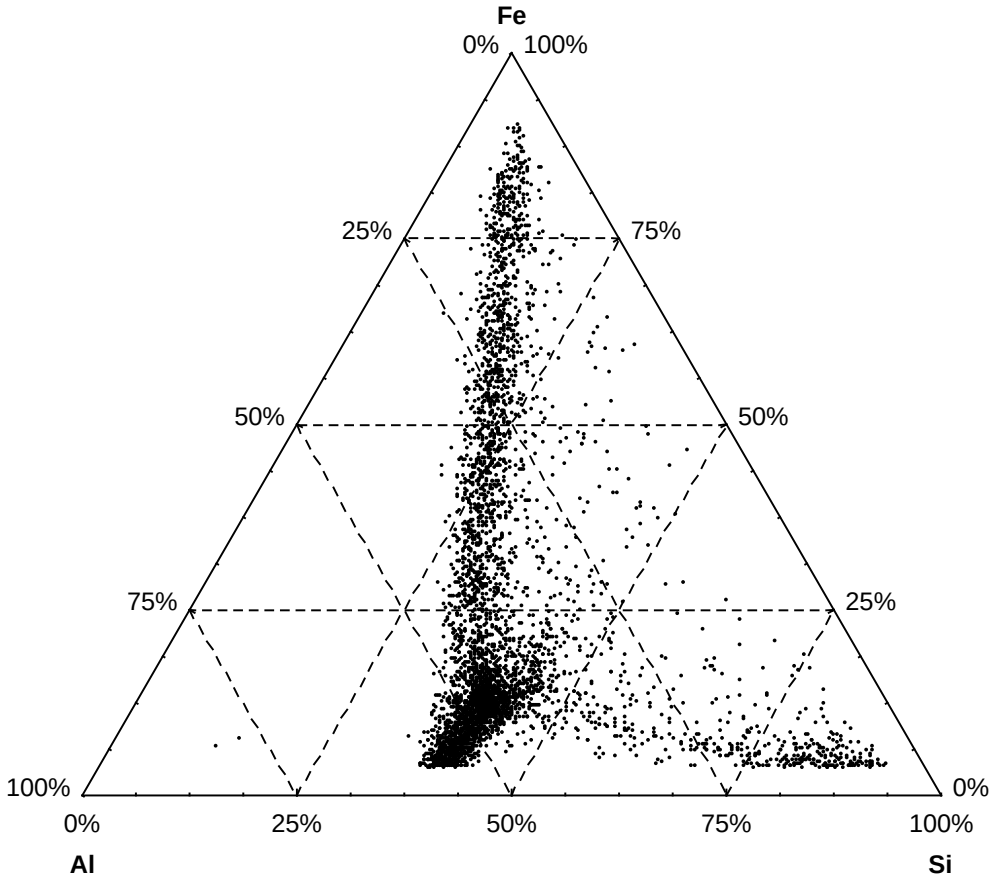

Figure 5-25: Ternary graph of Al, Si, and Fe for Class 30 particles within Burkina Soil 12A. The total number of particles plotted was 4,135 of the 7,856 particles analyzed.

Burkina Laterite 0

Burkina Laterite 0 was mainly comprised of the following classes: 3, 30, 37, 40, and 100. Approximately 56.0% of the particles analyzed were class 30 or Al-Si-Fe particle which was typical of the ratios seen in the soils analyzed. The next highest percentage of particles fell into the class 37 or Al-Si-K-Fe group. Burkina Laterite 0 was the only laterite which possessed any class 17 or Fe-Si particles and had 11.7% fall into this category. Lastly, Burkina Laterite 0 had a reasonably high percentage of class 3 or Fe particles with 9.4% whereas this particle class is of minor significance if not missing in the other laterites analyzed. Figure 5-26 illustrates somewhat typical trending of particles within class 30 for the Burkina soils.

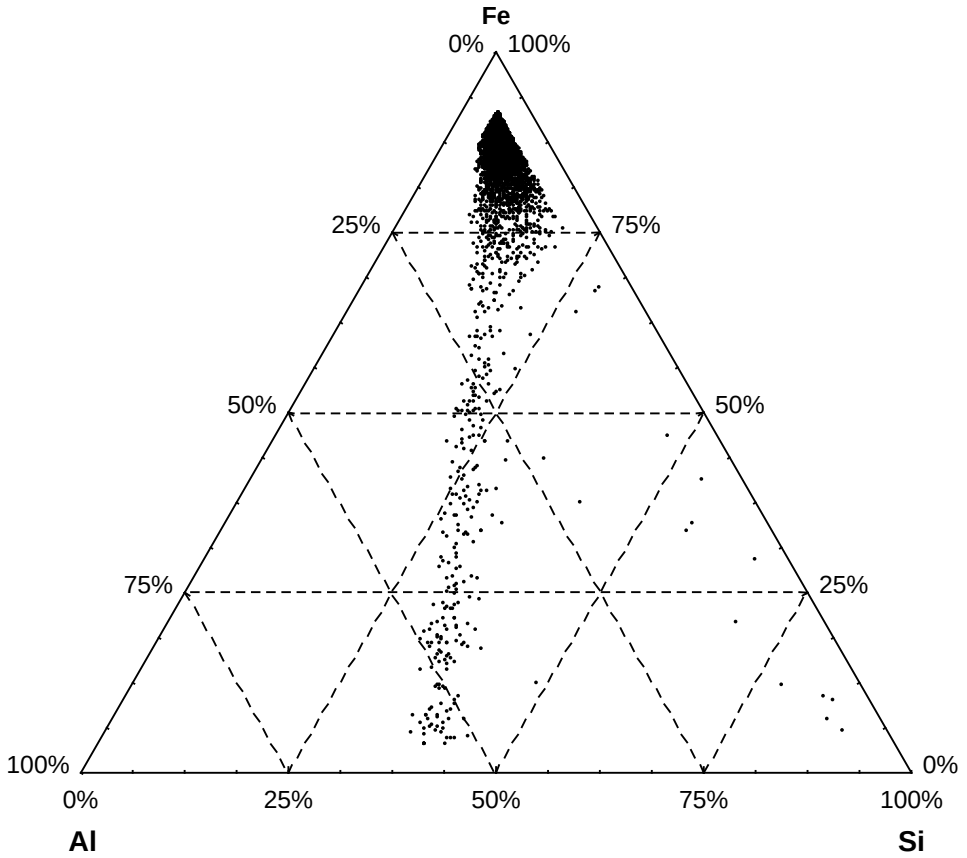

Figure 5-26: Ternary graph of Al, Si, and Fe for Class 30 particles within Burkina Laterite 0. The total number of particles plotted was 3,760 of the 6,713 particles analyzed.

Burkina Laterite 1

Burkina Laterite 1 was mostly comprised of the following classes: 8, 30, and 57. Approximately 90.9% of the particles analyzed were class 30 or Al-Si-Fe particle which was the highest of ratios seen in all the sediment samples analyzed. The next highest percentage of particles fell into the class 57 or Ti particles with 4.2%. Lastly, Burkina Laterite 1 possessed 1.3% particles which belonged to class 8 or Al-Si. Figure 5-27 illustrates somewhat typical linear trending of particles within class 30 for the Burkina Laterites. Although, laterites plotted typically showed the majority of particles had higher ratios of Fe for this class than what is seen in Burkina Laterite 1.

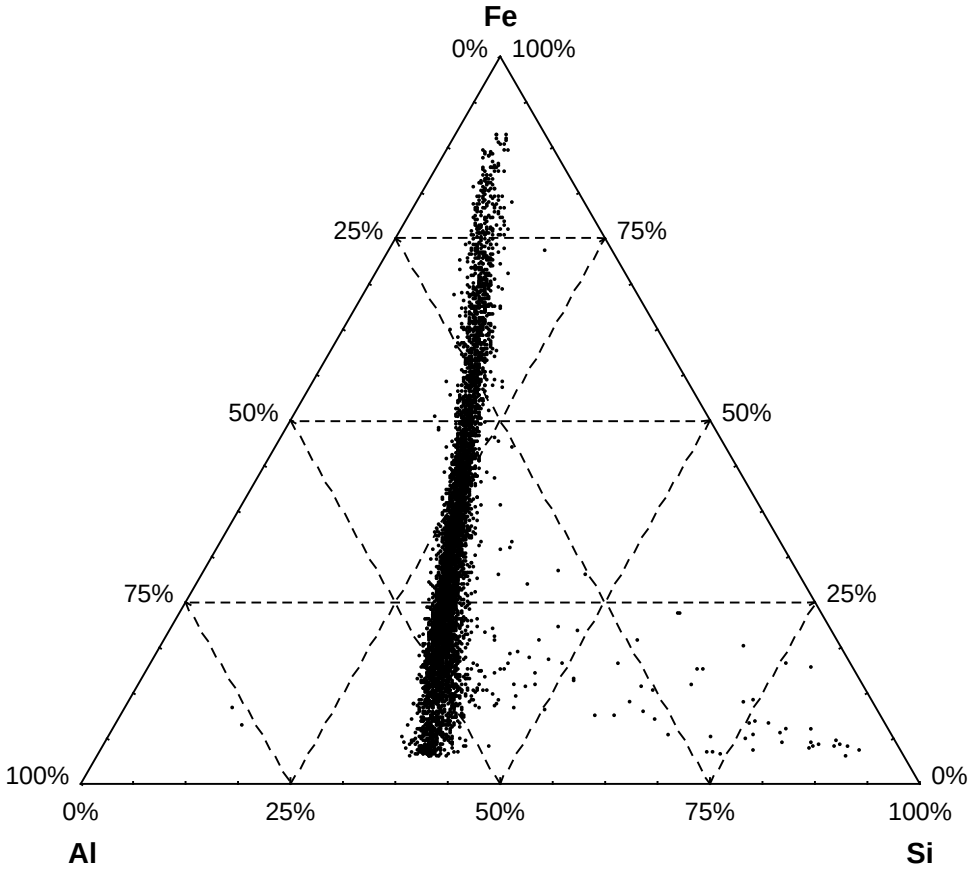

Figure 5-27: Ternary graph of Al, Si, and Fe for Class 30 particles within Burkina Laterite 1. The total number of particles plotted was 5,508 of the 6,063 particles analyzed.

Burkina Laterite 3

Burkina Laterite 3 was mainly comprised of the following classes: 1, 8, 9, 30, 31, and 37. Only 54.5% of the particles analyzed were class 30 or Al-Si-Fe particle which was the lowest of ratios seen in all the sediment samples analyzed and is more typical of percentages seen in soils than laterites. The next highest percentage of particles fell into the classes 8 and 9 with a combined percentage of 14.7% which again is more typical of what is seen in the soils analyzed. Additionally, Burkina Laterite 3 was comprised of 6.8% class 37 or Al-Si-K-Fe particles. Lastly, analyses revealed the presence of approximately 3.9% of class 1 or Si particles which was the highest percentage of any laterites. Figure 5-28 illustrates a particle distribution more typical of Burkina Soils analyzed with the majority of particles being composed of less than 50% Fe and higher ratios of Al and Si.

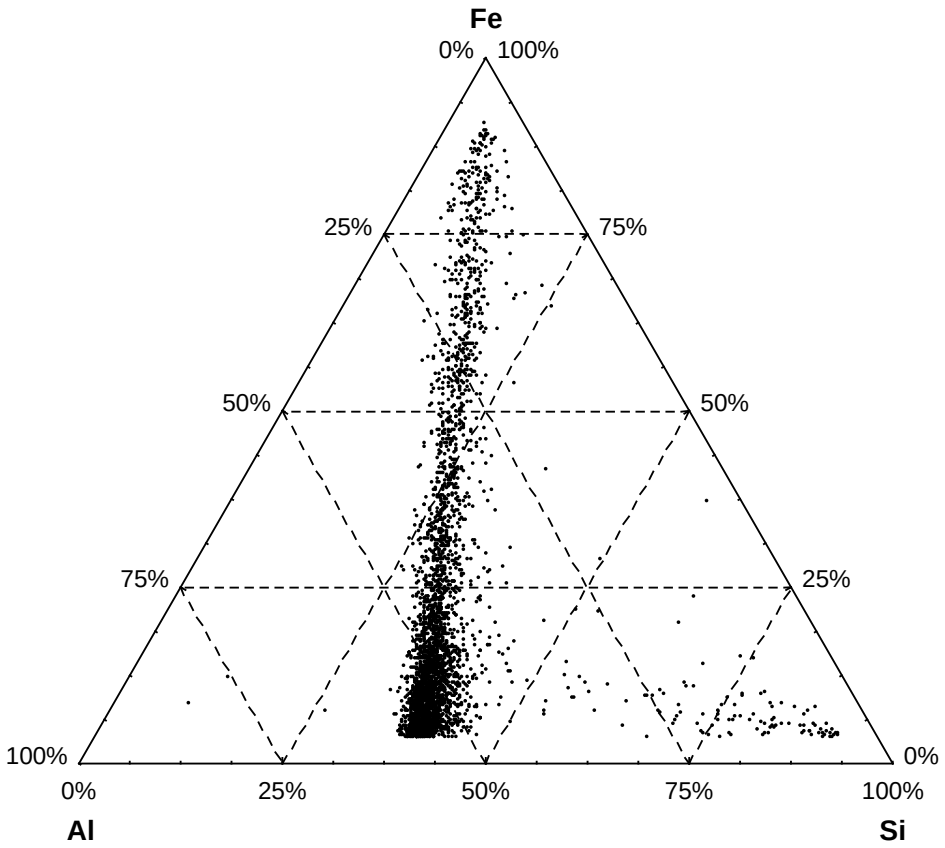

Figure 5-28: Ternary graph of Al, Si, and Fe for Class 30 particles within Burkina Laterite 3. The total number of particles plotted was 3,171 of the 6,025 particles analyzed.

Burkina Laterite 4

Burkina Laterite 4 was mostly comprised of the following classes: 3, 30, 35, 37, and 49. Approximately 83.2% of the particles analyzed were class 30 or Al-Si-Fe which was well within the range typically seen in laterites analyzed. The next highest percentage of particles fell into class 37 or Al-Si-K-Fe particles with 7.1%. Analyses also revealed the presence of approximately 1.3% of class 3 or Fe particles making Burkina Laterite 4 one of only three laterites to have this class. Finally, 1.0% of particles fell into class 49 or Na-Al-Si-Ca-Fe which was not seen in any other laterite analyzed. Figure 5-29 illustrates a linear particle distribution typically seen in Burkina Laterites analyzed with the majority of particles being composed of greater than 50% Fe.

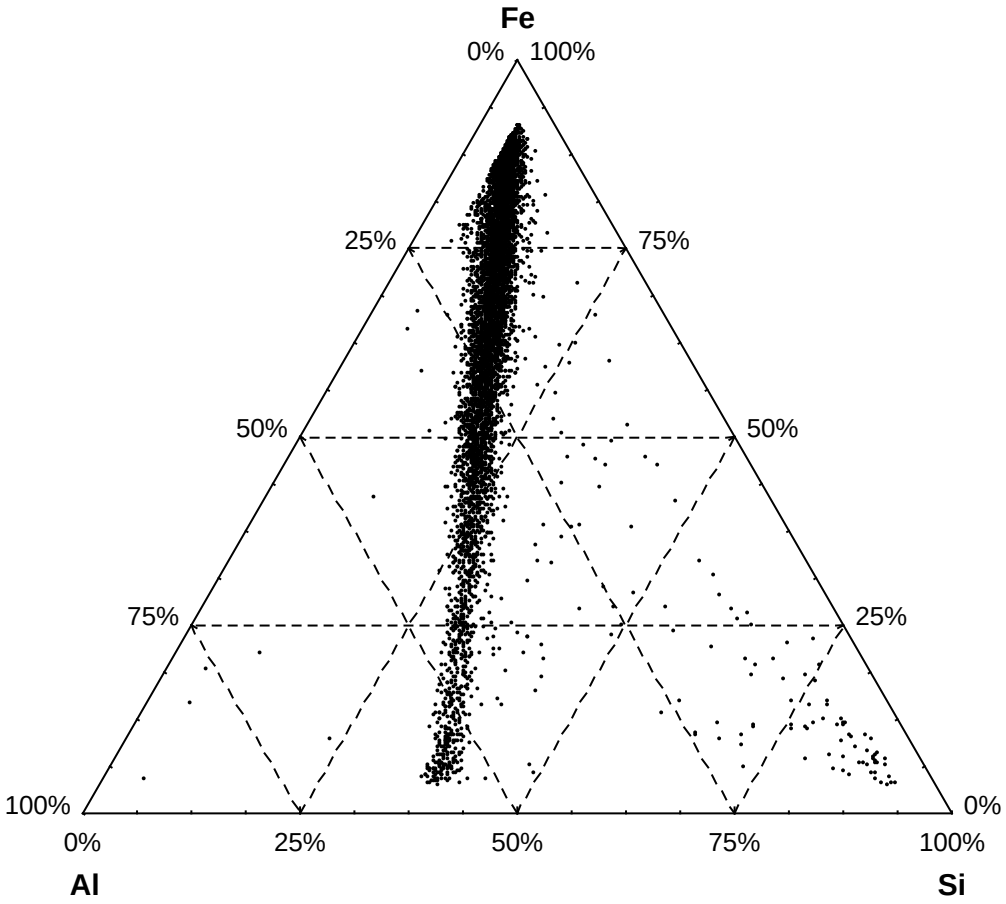

Figure 5-29: Ternary graph of Al, Si, and Fe for Class 30 particles within Burkina Laterite 1. The total number of particles plotted was 5,508 of the 6,063 particles analyzed.

Burkina Laterite 5

Burkina Laterite 5 was comprised of the fewest classes including only 30, 37, and 57. Approximately 78.2% of the particles analyzed were class 30 or Al-Si-Fe which was again typical of what was seen in laterites analyzed. The second highest percentage of particles fell into class 57 or Ti particles with 10.3% and was the highest percentage seen in all sediment samples analyzed. Third, analyses revealed the presence of approximately 7.6% of class 37 or Al-Si-K-Fe particles. Figure 5-30 illustrates a linear particle distribution typically seen in Burkina Laterites analyzed with the majority of particles being composed of greater than 50% Fe.

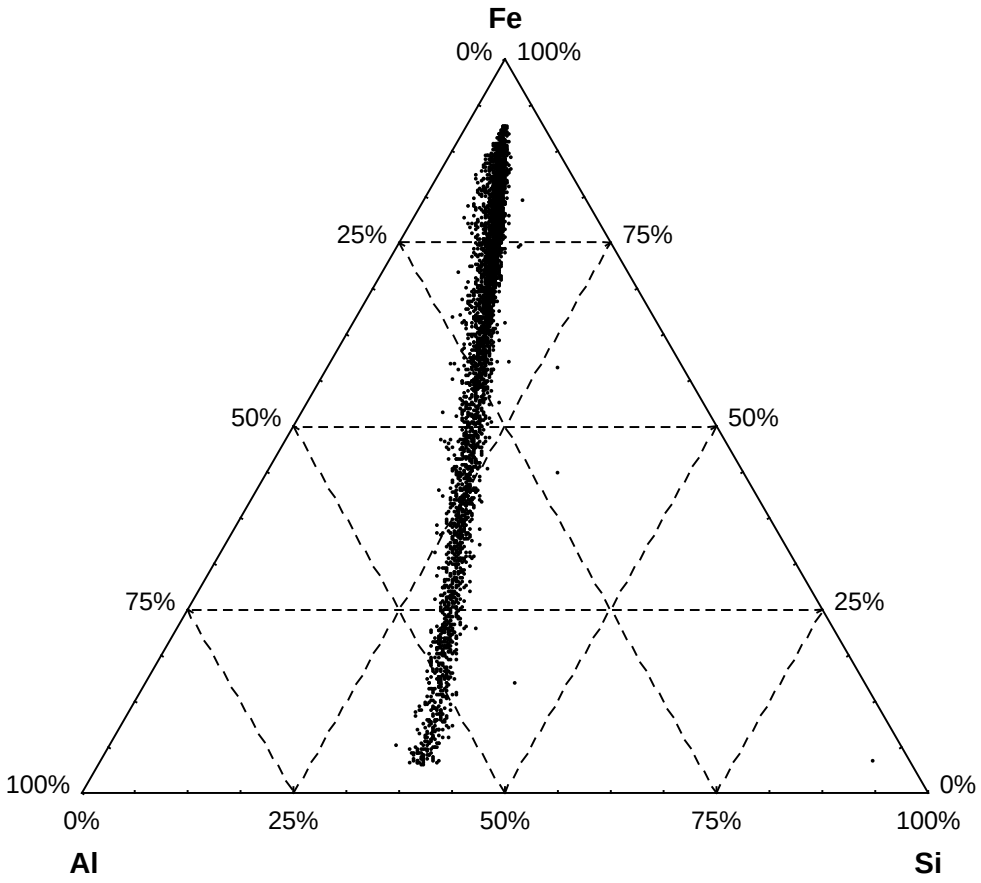

Figure 5-30: Ternary graph of Al, Si, and Fe for Class 30 particles within Burkina Laterite 5. The total number of particles plotted was 3,518 of the 4,502 particles analyzed.

Burkina Laterite 7

Burkina Laterite 7 was comprised of only five classes including 30, 35, 37, 57, and 58. Approximately 72.5% of the particles analyzed were class 30 or Al-Si-Fe. The next highest percentage of particles fell into class 35 or Na-Al-Si-Fe particles with 8.5%. A close second was class 37 or Al-Si-K-Fe particles with 7.1%. Burkina Laterite 7 also possessed a moderate amount, roughly 2.3%, of class 57 or Ti particles. Lastly, 1.5% of particles fell into class 58 or Mn >4% particles which was not seen in any other laterite analyzed. Figure 5-31 illustrates a linear particle distribution typically seen in Burkina Laterites analyzed with a somewhat gradual transition of Fe richness. The majority of particles plotted fell between 25% to 75% of Fe relative to Al and Si.

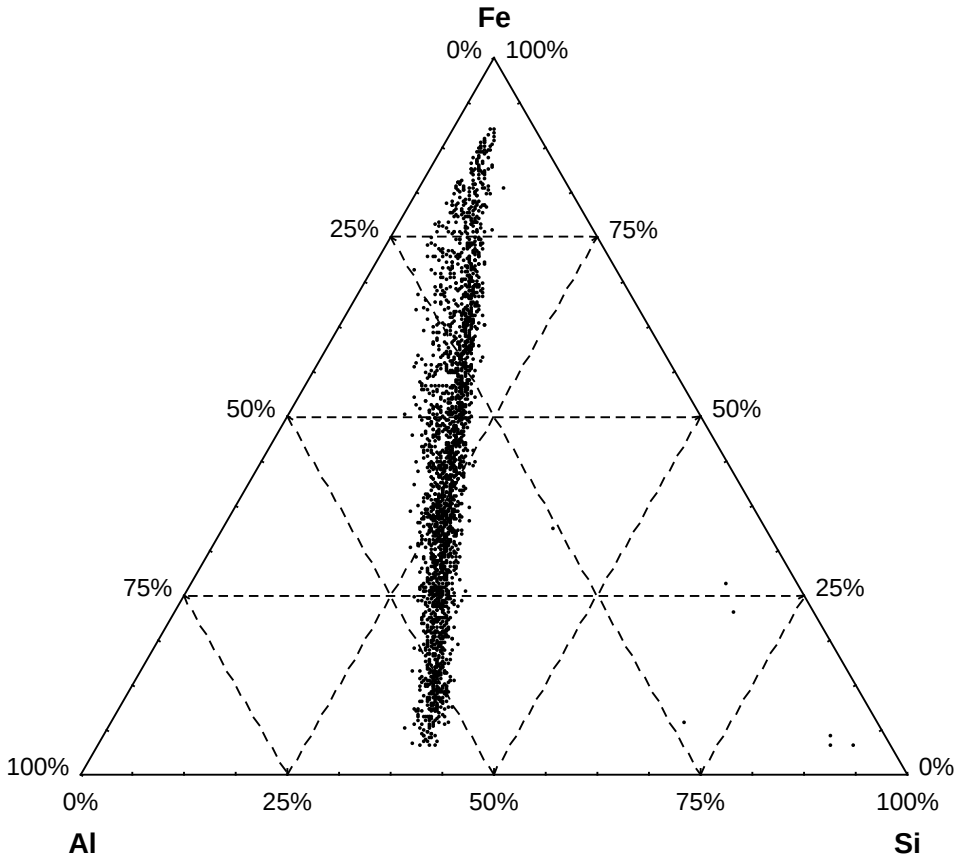

Figure 5-31: Ternary graph of Al, Si, and Fe for Class 30 particles within Burkina Laterite 7. The total number of particles plotted was 2,276 of the 3,140 particles analyzed.

Burkina Laterite 8

Burkina Laterite 8 was the most diverse in composition for all laterites analyzed and was composed of the following classes: 1, 8, 9, 30, 31, 34, 37, 57 and 100. Approximately 70.1% of the particles analyzed were class 30 or Al-Si-Fe. The next highest percentage of particles fell into classed 8 and 9 or Al-Si particles with approximately 8.6%. Thirdly, analyses revealed the presence of approximately 3.9% of class 37 or Al-Si-K-Fe. Burkina Laterite 8 also had a relatively high percentage of class 57 or Ti particles at 3.4% which was the third highest for all laterites analyzed. Additionally, 2.5% of particles were class 31 or Al-Si-K which only appeared in two laterites. Finally, approximately 4.0% of particles fell into class 100 or particles which were not classified in the linear sorting scheme. This was the highest percentage seen in all laterites. Figure 5-32 illustrates a somewhat linear particle distribution with a minor amount of particles straying from the trend.

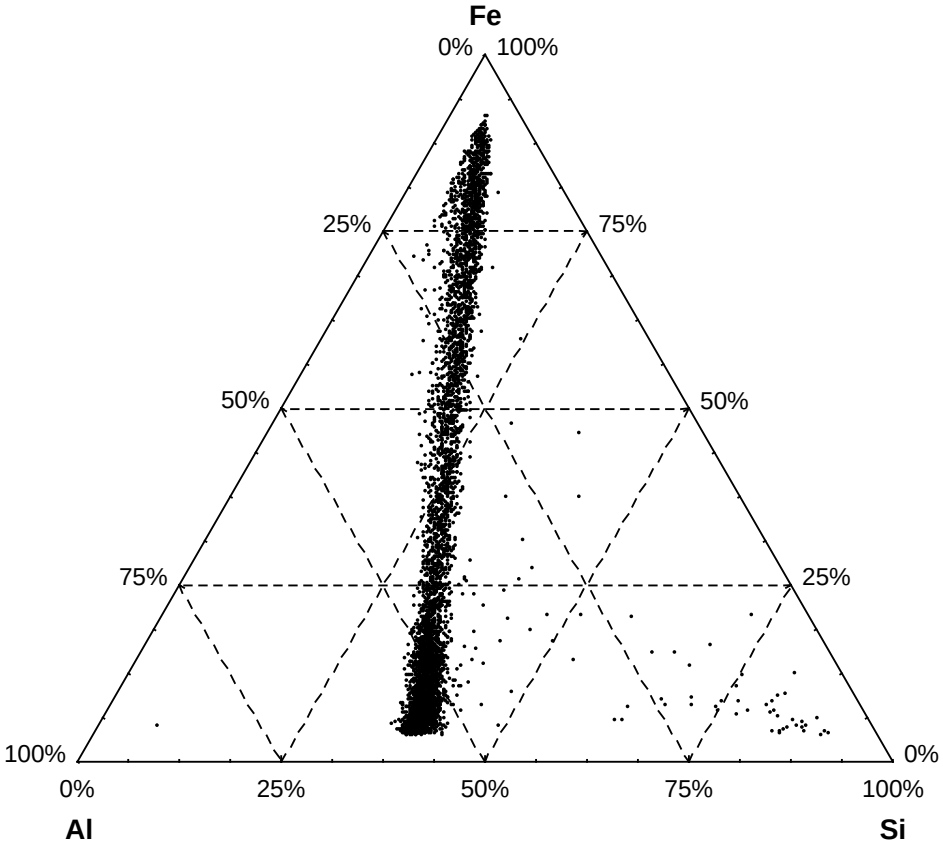

Figure 5-32: Ternary graph of Al, Si, and Fe for Class 30 particles within Burkina Laterite 8. The total number of particles plotted was 4,341 of the 6,212 particles analyzed.

Burkina Laterite 9

Burkina Laterite 9 was comprised of the following classes: 30, 35, 37, and 100. Approximately 87.5% of the particles analyzed were class 30 or Al-Si-Fe which was the third highest concentration seen in the laterites. The next highest percentage of particles fell into class 37 or Al-Si-K-Fe particles with 3.6%. Analyses also revealed the presence of approximately 1.4% of class 35 or Na-Al-Si-Fe particles. Lastly, 2.1% of particles fell into class 100 or particles not classified by the linear sorting scheme. Figure 5-33 illustrates a linear particle distribution typically seen in Burkina Laterites analyzed with the majority of particles being composed of less than 35% Si.

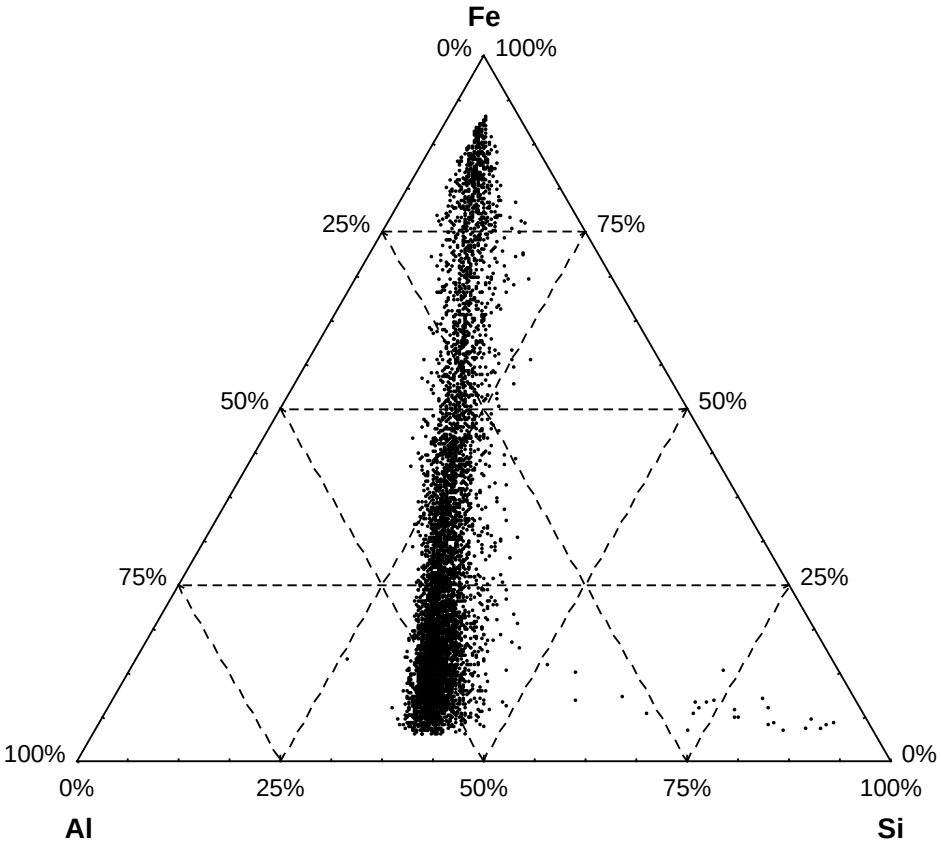

Figure 5-33: Ternary graph of Al, Si, and Fe for Class 30 particles within Burkina Laterite 9. The total number of particles plotted was 5,616 of the 6,414 particles analyzed.

Burkina Laterite 10

Burkina Laterite 10 was mostly comprised of the following classes: 3, 30, 35, 37, and 57. Of the particles analyzed, approximately 71.3% were class 30 or Al-Si-Fe. Class 35 or Na-Al-Si-Fe particles were the next highest percentage of particles with 14.9% which was the highest concentration seen for all laterites for this class. Analyses also revealed the presence of approximately 1.9% of class 3 or Fe particles making Burkina Laterite 10 one of only three laterites to have this class. Finally, 1.5% of particles fell into class 57 or Ti between 3 – 60%. Figure 5-34 illustrates a linear particle distribution typically seen in Burkina Laterites analyzed with the majority of particles being composed of less than 30% Si and greater than 50% Fe.

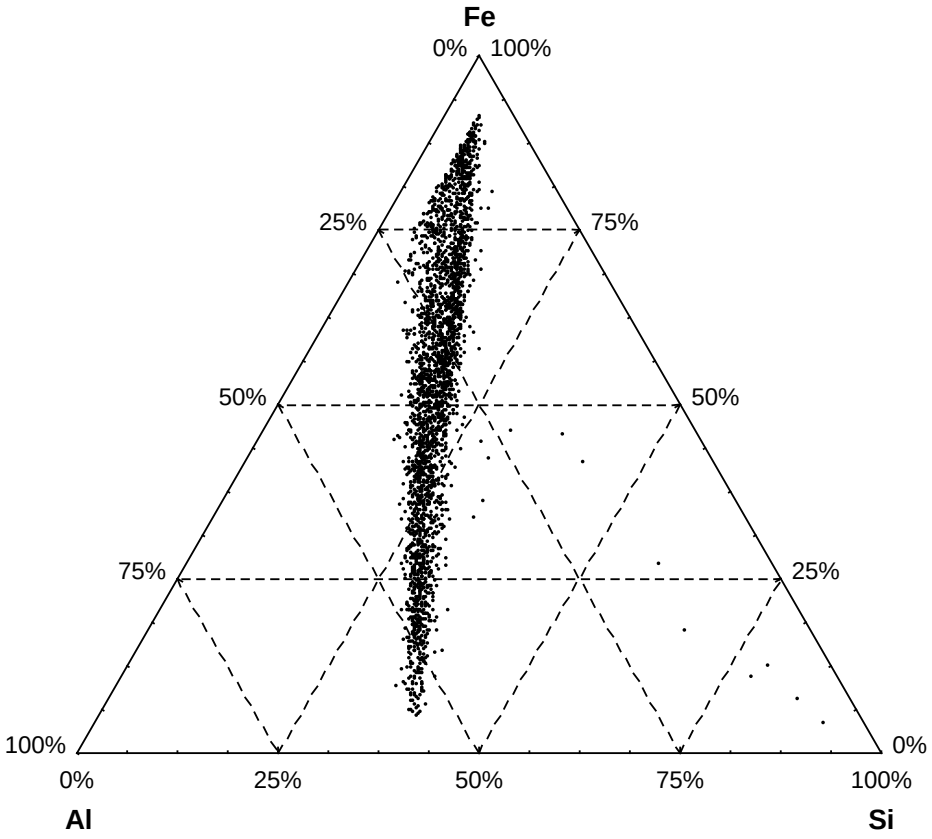

Figure 5-34: Ternary graph of Al, Si, and Fe for Class 30 particles within Burkina Laterite 10. The total number of particles plotted was 2,558 of the 3,422 particles analyzed.

Chapter 6

Conclusions

The investigation's results indicated sediment samples may be correlated to particular provenances based upon its unique constituent make up as well as constituent concentrations. Results also indicated that samples from the Burkina Faso and Niger regions are primarily composed of Al, Si, and Fe with varying and limited amounts of Ca, K, Mg, Mn, Na and Ti. Additionally, the data acquired indicated that the proposed linear classification scheme was adequate in sorting homogenous groups of particles and trending in the traits of particular classes was present.

Analysis of the Burkina Soils and Laterites indicated that class 30 or the Al-Si-Fe particles was of particular importance in sample and provenance identification. For soils, a modal composition of approximately 40-60% may be established for classification in the future whereas laterites typically had a modal composition of between 70-90%. Although relatively little research has been conducted on the regional sediment elemental composition, results for class 30 in laterites do correlate well with the lateritic profile conducted by Giorgis et al. 2013. What variation is present is likely due to the difference in bulk analysis and CCSEM analysis as well as the preceding classes of particles such as classes 3, 8, 9, and 17. In regards to distinguishing characteristics between soils and laterites, Si ratios for laterites are diminished in comparison to soils as a result of greater amounts of chemical weathering and dissolution or mobilization of silicate particles. The inverse was true for Fe ratios and much higher amounts could be seen in the results for class 30 as well as in FOV analysis.

Third, ternary plots of class 30 illustrated the difference in trends of these particles for soils and laterites. Soils demonstrated a somewhat more sporadic pattern than what was seen in the laterites and significant amounts of particles possessed less than 25% Fe being plotted more closely along the Al-Si axis. However, laterites typically yielded a more linear trend with a greater density of particles being plotted together in regards to higher Fe percentages with the majority of particles possessing greater than 50% Fe. The aforementioned increasing density may likely be an indicator of laterite maturity due to greater chemical weathering. Trends seen in laterites, such as Burkina Laterite 4, may be the result of moderate to heavily weathered mature laterites whereas the trending seen in Burkina Laterite 8 may be indicative of less mature laterites. Additionally, the ternary plot of class 30 particles for Burkina Laterite 0 illustrated that the majority of particles possessed greater than

75%, which could be the result of being subjected to the most extensive amounts of chemical weathering. Also, Burkina Laterite 0 was the only laterite that possessed a significant amount of particles within class 3 or Fe particles at 9.4% 17 or Fe-Si particles at 11.7% which also could indicate extensive chemical weathering as even the moderate amounts of aluminum has been mobilized.

In addition to being able to distinguish soils from laterites based upon differences seen in class 30, differences in preceding classes were quite significant. As laterites differ from soil mainly due to percentages of silica present in varying forms (Norton, 1973), this difference was demonstrated in percentages of classes 1, 8, and 9. For the most part laterite samples analyzed were almost devoid of class 1 or Si particles. With exception Burkina Laterite 3 and 8, percentages for class 8 and 9 particles were 1% or less whereas soils yielded 5–25% for these classes with an average of approximately 12%. Again, although Burkina Laterite 3 was visually classified as a laterite, based upon the further CSEM analyses it is more likely a heavily weathered soil due to its higher percentages of class 1, 8, and 9 particles as well as the ternary plot of class 30 particles mimicking traits seen in other soils.

Overall, the linear classification scheme developed for CCSEM appears to be an effective means of soil friable sediment analysis. Additionally, analysis of neighboring regions surface sediments should be conducted to identify unique traits associated with each region and to further validate this method of analysis. Also, joint analysis of other sediment along with whole rock analysis could be of assistance in order to correlate results with other studies using bulk analysis methods.

Appendix A

Tabulated Results from CCSEM Analysis

Class Number	Burkina Soil 4A	Burkina Soil 5A	Burkina Soil 6A	Burkina Soil 7A	Burkina Soil 10A	Burkina Soil 11A	Burkina Soil 12A	Class Parameters
1	2.3%	5.9%	9.2%	2.3%	1.9%	1.8%	8.3%	Si > 98%
3	1.5%	2.1%		1.4%		2.9%		Fe > 98%
6						2.5%		Ti > 60%
8	24.5%	1.8%	2.1%	3.7%	5.4%	3.9%	3.6%	SiAl > 98% and Si < 50%
9	1.6%	3.8%	15.2%	1.8%	4.2%	1.7%	12.6%	SiAl > 98% and Si > 75%
17				1.0%		1.1%		FeSi > 98%
30	48.7%	51.2%	43.6%	43.6%	51.4%	58.1%	52.6%	AlSiFe > 98% and Al > 3% and Si > 3% and Fe > 3%
31	4.0%	2.7%	5.5%	5.0%	1.0%		4.5%	AlSiK > 98% and Al > 3% and Si > 3% and K > 3%
33				1.8%			0.7%	AlSiNa > 98% and Al > 3% and Si > 3% and Na > 3%
35		4.4%	2.1%	7.8%	14.3%	1.1%		NaAlSiFe > 98% and Na > 3% and Al > 3% and Si > 3 % and Fe > 3%
36			1.0%		1.0%		0.6%	NaAlSiK > 98% and Na > 3% and Al > 3% and Si > 3 % and K > 3%
37	5.9%	7.3%	4.9%	6.5%	3.8%	11.4%	5.0%	AlSiKFe > 98%
38		1.1%				1.8%		AlSiFeMg > 98%
39						4.6%		AlSiFeP > 98%
47		2.7%		2.9%	1.3%	1.0%	0.8%	MgAlSiKFe > 98% and Mg > 3% and Al > 3% and Si > 3% and K > 3% and Fe > 3%
49			1.4%		1.7%			NaAlSiCaFe > 98% and Na > 3% and Al > 3% and Si > 3% and Ca > 3% and Fe > 3%
51		1.5%		2.5%	1.7%	1.0%	1.0%	NaAlSiKFe > 98% and Na > 3% and Al > 3% and Si > 3% and K > 3% and Fe > 3%
57	3.8%	4.1%	9.0%	6.3%	3.4%		3.3%	Ti > 3% and < 60%
58				2.0%	1.3%		0.6%	Mn > 4%
100	1.5%	3.6%		6.1%	1.0%	6.9%	4.0%	Non-classified
Total Particle Count	3240	2925	5194	3132	2061	5767	7856	

Class Number	Burkina Laterite 0	Burkina Laterite 1	Burkina Laterite 3	Burkina Laterite 4	Burkina Laterite 5	Burkina Laterite 7	Burkina Laterite 8	Burkina Laterite 9	Burkina Laterite 10	Class Parameters
1	0.4%		3.9%				1.0%			Si > 98%
3	9.4%			1.3%					1.9%	Fe > 98%
8		1.3%	12.2%				6.3%			SiAl > 98% and Si < 50%
9		0.7%	2.5%				2.3%			SiAl > 98% and Si > 75%
17	11.7%									FeSi > 98%
30	56.0%	90.9%	54.5%	83.2%	78.2%	72.5%	70.1%	87.5%	71.3%	AlSiFe > 98% and Al > 3% and Si > 3% and Fe > 3%
31			2.0%				2.5%			AlSiK > 98% and Al > 3% and Si > 3% and K > 3%
34							1.0%			NaAlSiCa > 98% and Na > 3% and Al > 3% and Si > 3 % and Ca > 3%
35	0.6%		3.1%	1.2%		8.5%	0.7%	1.4%	14.9%	NaAlSiFe > 98% and Na > 3% and Al > 3% and Si > 3 % and Fe > 3%
37	15.8%	0.8%	6.8%	7.1%	7.6%	7.1%	3.9%	3.6%	6.3%	AlSiKFe > 98%
40	1.4%									AlSiFeCa > 98% and Al > 3% and Si > 3% and Fe > 3% and Ca > 3%
49	0.7%			1.0%						NaAlSiCaFe > 98% and Na > 3% and Al > 3% and Si > 3% and Ca > 3% and Fe > 3%
57		4.2%			10.3%	2.3%	3.4%	0.8%	1.5%	Ti > 3% and < 60%
58						1.5%				Mn > 4%
100	1.3%						4.0%	2.1%		Non-classified
Total Particle Count	6713	6063	6025	6944	4503	3140	3998	6415	3422	

Appendix B

Bar Graphs of CCSEM Analysis Results

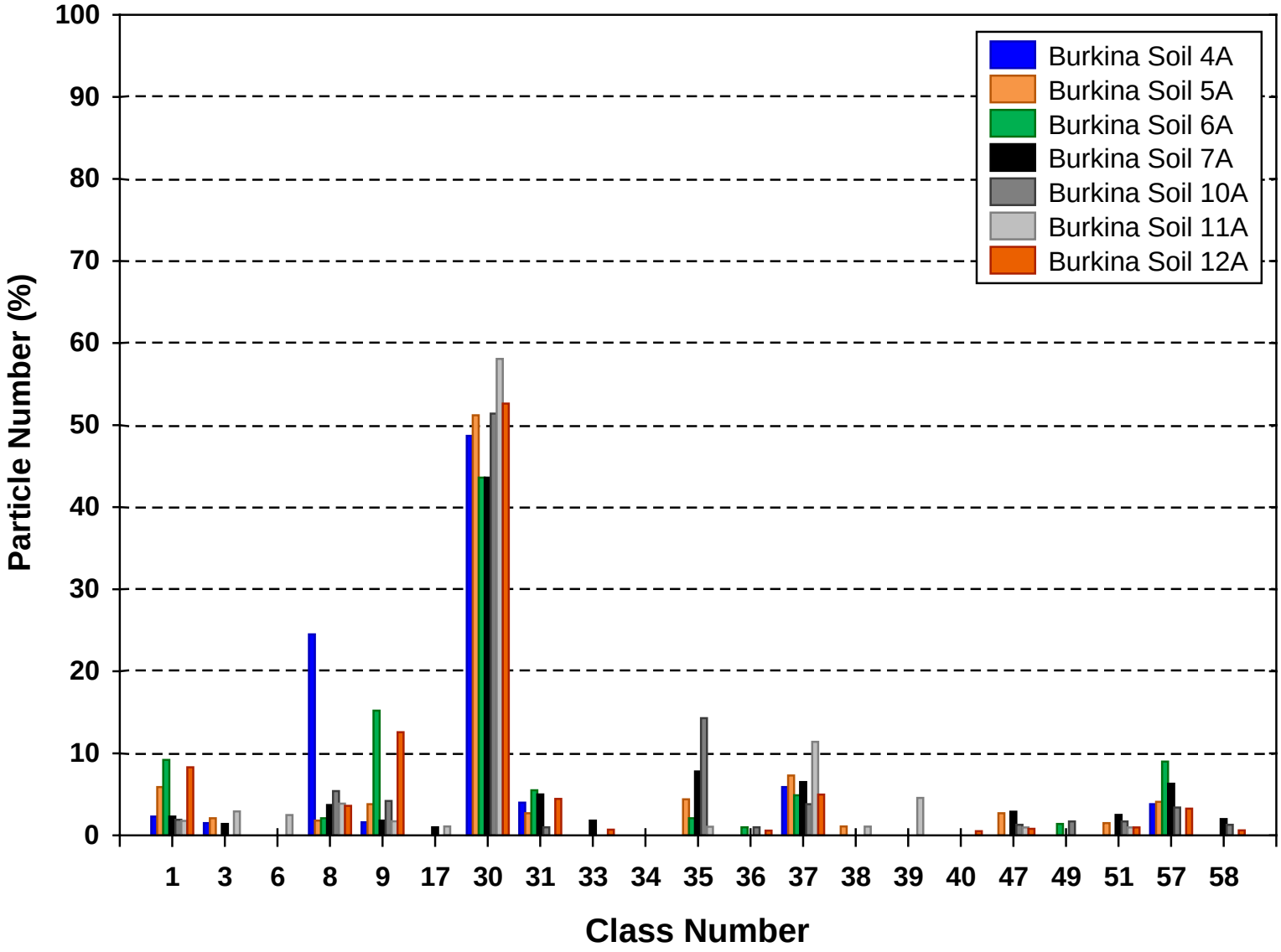
Burkina Soil 4A
Burkina Soil 5A
Burkina Soil 6A
Burkina Soil 7A
Burkina Soil 10A
Burkina Soil 11A
Burkina Soil 12A
Particle Number (%)
100
90
80
70
60
50
40
30
20
10
0
1
3
6
8
9
17
30
31
33
34
35
36
37
38
39
40
47
49
51
57
58
Class Number

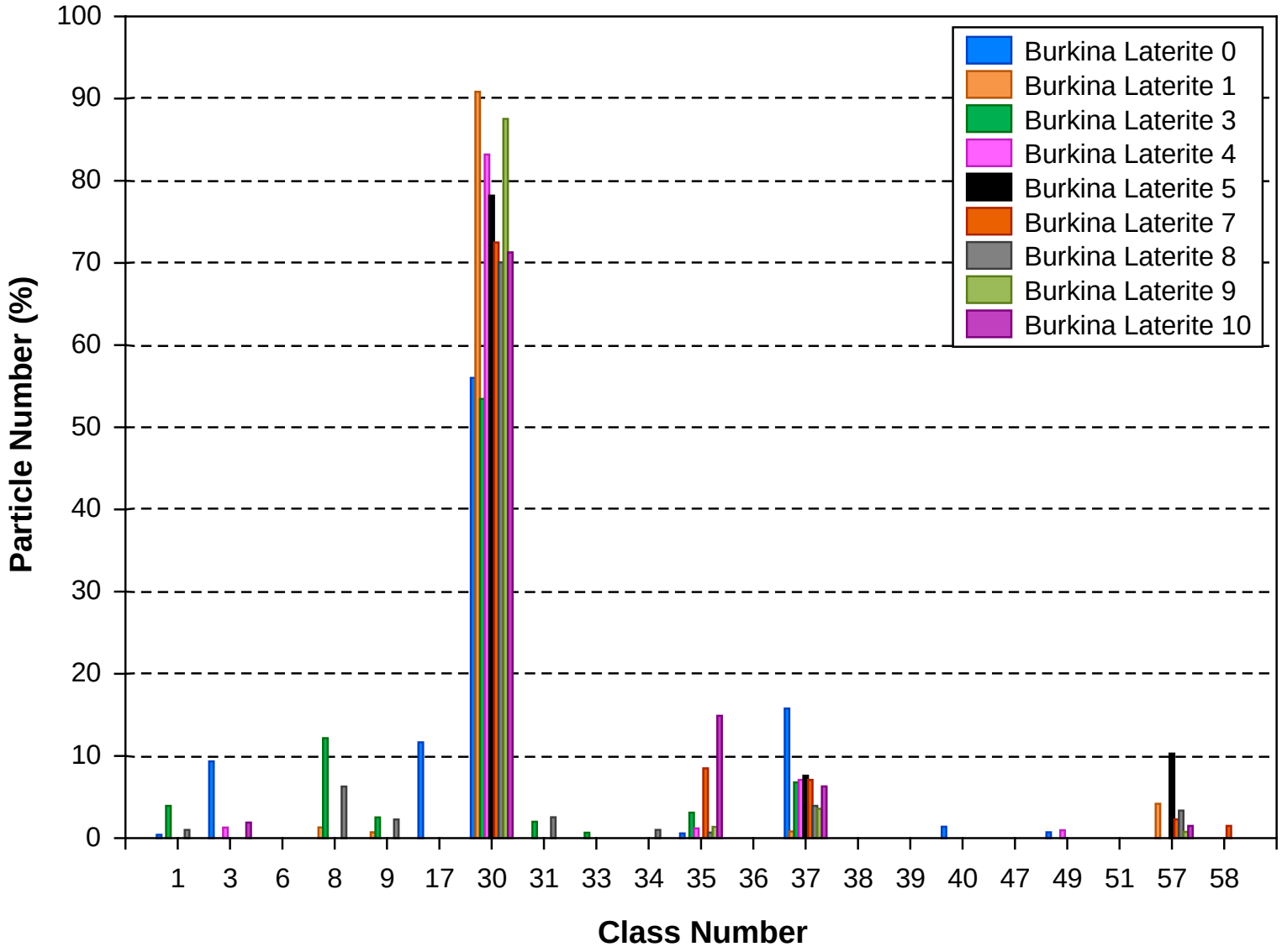
Particle Number (%)
100
90
80
70
60
50
40
30
20
10
0
1
3
6
8
9
17
30
31
33
34
35
36
37
38
39
40
47
49
51
57
58
Class Number
Burkina Laterite 0
Burkina Laterite 1
Burkina Laterite 3
Burkina Laterite 4
Burkina Laterite 5
Burkina Laterite 7
Burkina Laterite 8
Burkina Laterite 9
Burkina Laterite 10

References

Avila, A., Queralt-Mitjans, I., Alarcon, M. 1997. Mineralogical Composition of African Dust Delivered by Red Rains Over the Northeastern Spain, *J. Geophys. Res,* 102, 21 977–21 996.

Bartholet, J. 2012. Swept From Africa to the Amazon, *Scientific American*, 45-49.

Bennet, C.M., McKendry, I.G., Kelly, S., Denike, K., Koch, T. 2006. Impact of the 1998 Gobi Dust Event on Hospital Admission in the Lower Fraser Valley, British Columbia, *Sci. Tot. Environ.* 366, 918-925.

Blanco, A., De Tomasi, F., Fillippo, E., Manno, D., Perrone, M.R., Serra, A., Tafuro, A.M., Tepore, A. 2003. Characterization of African Dust Over Southern Italy, *Atmos. Chem. Phys. Discuss*, 3, pp. 1-38.

Coz, A., Andrés, A., Soriano, S., Viguri, J. R., Ruiz, M. C., Irabien, J. A. 2009. Influence of Commercial and Residual Sorbents and Silicates as Additives on the Stabilisation/Solidification of Organic and Inorganic Industrial Waste, *Journal of Hazardous Materials*, 164, 755–761.

Cos, E., Moreno, T., Artinano, B. 2011. Variations on the Mineralogical Particle Properties of Atmospheric Saharan Dust from Different Source Regions. *Revista de la Sociedad Espanola de Mineralogia*, Macla 15, pp. 69-70.

“Dust to Gust”. EurekAlert!. AAAS. 28 December 2006. Retrieved 17 August 2014.

Falkovich, A.H., Schkolnik, G., Ganor, E., Rudich, Y., 2004. Adsorption of Organic Compounds Pertinent to Urban Environments onto Mineral Dust Particles. *J. Geophys. Res*. 109, D02208. doi:10.1029/2003JD003919.

Formenti, P., Shutz, Y., Desboeufs, K., Ebert, M., Kandler, K., Petzold, A., Scheuvens, D., Weinbruch, S., Zhang, D. 2011. Recent Progress in Understanding Physical and Chemical Properties of African and Asian Mineral Dust. Atmos. Chem. Phys., 11, 8231-8256, doi: 10.5194/acp-11-8231-2011.

Giorgis, I., Bonetto, S., Giustetto, R., Lawane, A., Pantet, A., Rossetti, P., Thomassin, J., Vinai, R. 2013. The lateritic profile of Balkouin, Burkina Faso: Geochemistry, mineralogy and genesis. Journal of African Earth Sciences, 90, 31-48.

Goudie, A.S., Middleton, N.J., 2001. Saharan Dust Storms: Nature and Consequences, *Earth-Sci. Rev*., 179-204.

Intergovernmental Panel on Climate Change (IPCC). 2007. Available from: <http://www.ipcc.ch/pdf/assessment-report/ar4/syr/ar4_syr.pdf>.

Krech, S., McNeill, J.R., Merchant, C., Jump Up. Encyclopedia of World Environmental History. Routledgw. Pp. 748-749. ISBN 0-415-93734-5

Lyons, R., Oldfield, F., Williams, E. 2010. Mineral Magnetic Properties of Surface Soils/Sands Across Four North African Transects and Links to Climatic Gradients, Geochemistry, Geophysics, Geosystems, vol 11, issue 8, doi: 10.1029/2010GC003183.

Lyons, R., Oldfield, F., Williams, E. 2011. The Possible Role of Magnetic Measurements in the Discrimination of Sahara/Sahel Dust Sources, Earth Surface Processes and Landforms, vol 37, doi: 10.1002/esp.2268.

Mahowald, N.M., Baker, A.R., Bergametti, G., Brooks, N., Duce, R.A., Jickells, T.D., Kubilay, N., Prospero, J.M., Tegen, I. 2005. Atmospheric Global Dust Cycle and Iron Inputs to the Ocean, *Global Biogeochem. Cy.*, 19, GB4025, doi: 10.1029/2004GB002402.

Mamane, Y., Ganor, E., Donagi, A.E., 1980. Aerosol Composition of Urban and Desert Origin in the Eastern Mediterranean I: Individual Particle Analysis. *Water Air Soil Pollut.* 14, 29–43.

Mather, R.L., Reynolds, S.E., Wolff, G.A., Williams, R.G., Torre-Valdes, S., Woodward, E.M.S., Landolfi, A., Pan, X., Sanders, R., Achterberg, E.P. 2008. Phosphorus Cycling in the North and South Atlantic Ocean Subtropical Gyres, *Nature Geoscience*, 1, 439-443.

Mormon, S., Plumlee, G. 2013. The Role of Airborne Mineral Dusts in Human Disease, *Aeolian Research 9*, 203-212.

Norton, S. A., 1973. Laterite and Bauxite Formation, Economic Geology, 68, 353-361.

Plumlee, G.S., Morman, S.A., Ziegler, T.L. 2006. The Medical Geochemistry of Dusts, Soils, and Other Earth Materials: Invited. In: Lollar, G.S. (Ed.), Treatise on Geochemistry, vol. 9, Elsevier, pp. 1-61.

Prospero, J.M., Glaccum, R.A., Nees, R.T. 1981. Atmospheric Transport of Soil Dust from Africa to South America, *Nature*, 289, 570-572.

Prospero, J.M., 1999. Long-Range Transport of Mineral Dust in the Global Atmosphere: Impact of African Dust on the Environment of the Southeastern United States, *Proc. Natl. Acad. Sci.* USA, 96, 3396-3403.

Shultz, H., Brand, P., Heyder, J. 2000. Particle Deposition in the Respiratory tract. In: Gehr, Peter, Heyder, Joachim (Eds.), Particle-Lung Interactions. Lung Biology in Health and Disease, vol. 143. Marcel Dekker, Inc., New York, pp. 229-277.

Sullivan, R.C., Guazzotti, S.A., Sodeman, D.A., Tang, Y., Carmichael, G.R., Prather, K.A., 2007. Mineral Dust is a Sink for Chlorine in the Marine Boundary Layer. *Atmos. Environ.* 41, 7166–7179.

United States Enviromental Protection Agency (USEPA). 2012a. Particulate Matter. Available from: http://www.epa.gove/airquality/particlepollution/

World Health Organization (WHO). 2012a. Available from: http://www.who.int/mediacentre/factsseet/fs313/en/